THESIS FOR THE DEGREE OF DOCTOR OF PHILOSOPHY IN SOLID AND STRUCTURAL MECHANICS

Ductile damage modeling of the machining process

SENAD RAZANICA

Department of Industrial and Materials Science
Division of Material and Computational Mechanics
CHALMERS UNIVERSITY OF TECHNOLOGY

Göteborg, Sweden 2019

Ductile damage modeling of the machining process

SENAD RAZANICA
ISBN 978-91-7597-884-0

Doktorsavhandlingar vid Chalmers tekniska högskola
Ny serie nr. 4565
ISSN 0346-718X
Department of Industrial and Materials Science
Division of Material and Computational Mechanics
Chalmers University of Technology
SE-412 96 Göteborg
Sweden
Telephone: +46 (0)31-772 1000

Cover:
Ductile failure modes at different stages in the deformation process of a hollow sheet with representative contours of the effective plastic strain.

Chalmers Reproservice
Göteborg, Sweden 2019

Ductile damage modeling of the machining process

Thesis for the degree of Doctor of Philosophy in Solid and Structural Mechanics
SENAD RAZANICA
Department of Industrial and Materials Science
Division of Material and Computational Mechanics
Chalmers University of Technology

Abstract

Machining processes are among the most common manufacturing processes for producing components used on a daily basis. It is a complex material removal process. Today, the research and development within the manufacturing industry is addressed by cost efficient numerical simulation strategies rather than by costly experimental procedures. The numerical simulation tools must then be able to model material subjected to inelastic deformations at high strain-rates and elevated temperatures and use reliable and well defined models for ductile material behavior and fracture.

The development of the modeling strategy, for the ductile material and fracture response herein, is embedded in a continuum thermodynamics framework. The Johnson-Cook constitutive model is applied for the effective visco-plastic material response. The ductile fracture behavior, is modelled by a continuum damage enhanced material formulation where an inelastic damage threshold is followed by a damage evolution law. A set of smeared damage evolution models are proposed, which are shown to give mesh independent results for quasi-static and isothermal conditions.

In addition, for more general situations, an alternative continuum progressive ductile damage model coupled to thermodynamics is formulated, where the damage induced fracture area production is based on a progression speed and a length-scale parameter. The damage evolution is then governed by a damage driving energy which, defined from the dissipation rate, consists of both elastic and inelastic contributions. In this way, the model is able to represent the ductile fracture process in a thermodynamically consistent way at high strain-rates and elevated temperatures, while partly preserving the mesh independent response. Moreover, the ability of the model to capture the material and fracture response at various states of stress triaxiality is investigated and results are compared with experiments. The damage model is shown to be able to capture the fracture response with the appropriate formulation of the damage driving energy including at least the inelastic part.

Finally, the continuum progressive ductile damage model is applied in a rigid visco-plastic context for the simulation of the orthogonal machining process. Here, simulation results for the difficult-to-cut material Alloy 718 are compared with experimentally determined forces, tool-chip contact-lengths and chip shapes at varying cutting speeds. Even though the proposed damage model consists of few parameters it is able to represent the cutting parameters considered in good agreement with experiments.

Keywords: Machining simulation, Mesh dependence, Thermodynamics, Johnson-Cook, Ductile fracture, Damage threshold criterion, Damage evolution, Damage driving energy

To my dear parents and sister,
Alija, Aida and Sabina

Preface

The work presented in this thesis has been carried out during the years 2013-2018 at the Department of Industrial and Material Science, Division of Material and Computational Mechanics, Chalmers University of Technology. The research was financially supported by the Swedish national research program FFI (Strategic Vehicle Research and Innovation), subarea sustainable production and the Ekmanska Foundation (Ekmanska stiftelsen) which I would like to gratefully and sincerely thank. Some of the results presented in this thesis are based on simulations conducted on resources at Chalmers Center For Computational Science and Engineering (C3SE) provided by the Swedish National Infrastructure for Computing (SNIC).

Acknowledgements

First and foremost, I would like to express my sincere gratitude to my supervisors Prof. Ragnar Larsson and Prof. Lennart Josefson. Throughout these years and regardless of periods of success or setbacks, they have always maintained their patience and commitment while providing continuous support, invaluable guidance, knowledge and encouragement. Without your individual efforts and contributions, the thesis would have been difficult, if not impossible, to accomplish.

I would like to take the opportunity to thank the co-authors of the appended papers. Amir Malakizadi at the Division of Materials and Manufacture at Chalmers University of Technology for his flourishing contributions and interesting discussions regarding machining processes and simulations, material behaviour and not at least experimental procedures. Stefan Cedergren at GKN Aerospace for the excellent high resolution micro-structural photos of Alloy 718 material and discussions on metal cutting. Last but not the least, Torsten Sjögren at the Research Institutes of Sweden for his assistance and discussions regarding the experimental work on CGI.

I would also like to thank my colleagues at the Division of Material and Computational Mechanics and the Division of Dynamics at Chalmers University of Technology for creating a friendly environment and for plenty of interesting discussions. I would also like to thank, Goran Ljustina at Volvo Car Corporation for his mentorship during my first year as PhD student but as well for the interesting collaboration in the MCGUIDE project. At the same time, I would like to thank all remaining participants from Volvo, Scania CV, Sandvik Coromant and Royal Institute of Technology in the MCGUID project. Thank you all, you enabled me to connect the dots, as Steve Jobs once said, "between modeling, simulations and experiments".

Finally, I acknowledge with a deep sense of reverence, my gratitude towards my parents and sister, for their endless love, understanding, support and encouragement throughout all these years.

Gothenburg, March 2019
Senad Razanica

Thesis

This thesis consists of an extended summary and the following appended papers:

Paper A R. Larsson, S. Razanica and B.L. Josefson. Mesh objective continuum damage models for ductile fracture. *International Journal for Numerical Methods in Engineering* **106** (2015), 840–860. DOI: 10.1002/nme.5152

Paper B S. Razanica, R. Larsson and B. L. Josefson. A ductile fracture model based on continuum thermodynamics and damage. *Submitted for international publication*

Paper C S. Razanica, B. L. Josefson, R. Larsson and T. Sjögren. Validation of the ductile fracture modeling of CGI at quasi-static loading conditions. *To be submitted for international publication*

Paper D S. Razanica, A. Malakizadi, R. Larsson, S. Cedergren and B. L. Josefson. FE modeling of machining Alloy 718 using a novel ductile damage model. *To be submitted for international publication*

Contributions to the appended paper

Paper A

- Took part in the planning of the paper and the theoretical developments.
- Wrote the first draft of the paper while the final version was written in close collaboration with the co-authors.
- Performed the numerical implementation together with the co-authors and conducted the simulations.

Paper B

- Took part in the planning of the paper and the theoretical developments.
- Wrote the first draft of the paper while the final version was written in close collaboration with the co-authors.
- Performed the numerical implementation and most of the the simulations.

Paper C

- Planned and wrote the major part of the paper.
- Performed the numerical implementation and conducted the the simulations.
- Took part in the reevaluation of the experimental investigation

Paper D

- Took part in the theoretical developments.
- Responsible for the planning and writing of the first draft of the paper while the final version was written in close collaboration with the co-authors.
- The implementation in DEFORM 2D was done together with Amir Malakizadi, who also performed the simulations.
- Performed the specific experimental measurements presented in the paper.

Contents

Part I
Extended Summary

1 Introduction

1.1 Background and motivation

Machining is the most adopted metal shaping process in the manufacturing industry accounting for approximately 15 % of the value of all mechanical components worldwide [1]. Part of the explanation relate to its high precision, where a tolerance on a level of microns is readily achievable. The versatility of the process is another contributing factor. By applying machining processes, to form and shape complicated geometries, a vast amount of time and economical expenses can be reduced. The increasing competition in the manufacturing industry, where productivity, efficiency and ongoing development are key aspects striven for in order to be in the leading edge, has further favored the use of metal machining processes [2].

To continuously improve the key aspects within manufacturing industry a detailed understanding and development of the machining processes is of great importance. The research within the field has, so far, lead to e.g. advances in machine tools, optimization of machining operations and new cutting tools for a variety of materials and machining operations. However, the increased knowledge of the processes has enlightened other important aspects to be consider in order to continue accelerating the development.

Evidently, machining is a material removal process where a considerable waste of material- up to 10 % of the workpiece volume might be removed to reach the final geometrical dimensions [3]. With ever increasing demands on machined components/parts, the increased productivity from the manufacturing point of view is reflected in terms of an increasing material removal rate (cutting speed, feed and depth of cut). The increased removal rate result in increased thermo-mechanical loads, due to severe material deformation, on the cutting tool which lead to an increased wear of the tool and hence poor machining conditions. These conditions will significantly affect the product quality by altering the surface integrity e.g. the residual stresses at the surface and the mechanical properties of the final component. Hence, there are tremendous incentives to fine-tune existing manufacturing processes, or to replace them with new and innovative ones, in order to obtain near-net-shape. Therefore, it is important to optimize the whole manufacturing process, on a macro-level, with respect to distortion, surface integrity and operational conditions so that the productivity, efficiency and not least the product quality are secured.

To achieve this, the processing parameters on a micro-level, e.g. the creation of desirable compressive surface stresses, cutting forces, temperature and tool wear need to be controlled. These issues were previously addressed in the manufacturing industry via the application of costly experimental procedures in order to optimize the operational conditions based on the processing parameters. However, recently focus has shifted

towards a more cost efficient strategy concerning the implementation of simulation tools based on the finite element method (FEM) for the machining operations e.g. turning, milling and grinding included in the manufacturing chain [4], [5], [6]. Therefore, to represent the considered machining operations, the simulation tool needs to accurately represent the divesrity of physical phenomena that occur in the vicinity of the cutting tool. This concerns the modeling of e.g., large elasto-plastic deformations, high deformation rates including elevated temperatures that potentially might lead to adiabatic shear band formations and localized fracturing. In the case of machining heterogeneous materials, the interaction between different phases in the microstructure lead to an additional complexity of the deformation process [7]. It has been shown that the reliability of the modeling results are strongly coupled to the viability to the adopted constitutive model to accurately describe the material deformation [3], [8]. Hence, to simulate the machining operations the modeling of the ductile material and fracturing response is crucial but needs to be set in relation to the computational efficiency. For this emphasis most of the recent modeling approaches with respect to the ductile material and fracture behavior are derived within the local continuum framework. Unfortunately, these local continuum models experience a pathological mesh dependence if not a mesh objective enhancement or re-meshing technique is applied. The occurrence of the mesh dependence has been shown and investigated in relation to the modeling of machining processes e.g. [9], [10]. Therefore, it is of significant importance that the adopted modelling framework in the present thesis work is able to represent the material response mesh independently as possible.

Summarizing, to further contribute to the development of reliable simulation tools for optimization and understanding of the machining process, more efficient modeling approaches need to be considered. To achieve this, the number of calibration parameters for the material and damage models used need to be held on a realistic level, while still representing the physics in the cutting zone hence, reducing the need for time consuming and costly experimental testing. Additionally, the numerical modeling needs to be time efficient for industrial applications thus, developing the material and damage models within the continuum framework is an established and widely applied approach. Evidently implying that the inherited mesh dependence needs to be reduced to accurately model the process. If accomplished, the modeling strategy might potentially be adopted in industrial applications related to the machining process.

1.2 Purpose and aim

The purpose of the presented work stems from the need to efficiently, accurately and independently of operational material predict and optimize the operational conditions for machining processes. The aim of this thesis is to model the ductile material and fracture response so the purpose will be fulfilled.
To accomplish this, the following ***research questions*** are addressed:

- How is ductile damage characterized ?
- How should the pre- and post peak response be modelled to represent the ductile

FE-response and reduce the mesh dependence present in the local continuum framework?

- Which are the important material and failure phenomena necessary to be account for in order to simulate the machining process based on the FEM?
- How should the ductile damage model be incorporated for the simulation of the machining process?

1.3 Outline

The structure of this thesis is presented in this section. As a point of departure an overview of the modeling of ductile damage and machining is presented in section 2. Here the fundamental aspects of ductile damage and fracture are introduced and discussed together with relevant modeling approaches. Moreover, a general description of the machining process is introduced where important central aspects and modeling approaches are highlighted.

The modeling framework developed for the ductile material behavior and fracturing process is presented in section 3. The objective is to describe the ideas applied for the modeling, starting with a general description of the ductile material and fracturing process in section 3.1. It is followed by detailed description of the modeling approach adopted in section 3.2-3.4.3. These sections highlight the damage enhancement, the inelastic damage threshold criterion followed by the damage evolution described by a smeared and continuum damage evolution law derived in **Paper A** and **Paper B**, respectively. Finally, in section 3.4.5 the continuum damage evolution law developed in **Paper B**, is validated in **Paper C** with respect to the formulation of the damage driving energy at varying states of stress triaxiality where the main findings are highlighted.

The modeling framework adopted for the machining process, in **Paper D**, is presented in section 4. The incorporation of the ductile material damage and fracture modeling, from section 3, in a machining simulation context is described in section 4.2 - 4.3. The outcome and main results are presented and discussed in section 4.4. The thesis is finalized with a short summary of the appended papers in section 5 followed by concluding remarks in section 6 and an overview of future work in section 7.

2 Modeling overview of ductile damage and machining

Damage is in general governed by the mechanism of debonding however, depending on the considered material, loading conditions and thermal conditions that prevail, the process can be manifested in various ways. Ductile fracture, as illustrated in Figure 2.1, is often associated with significant amount of plastic deformation, where the nucleation of voids and micro-cracks grow and coalesce on a micro-structural level to form macroscopic cracks [11], [12]. This type of fracture is frequently occurring in engineering applications e.g. machining, automotive and aerospace. To be equipped to accurately and efficiently model ductile fracture, it is of significance to understand and be able to model and predict the underlying phenomena governing this process.

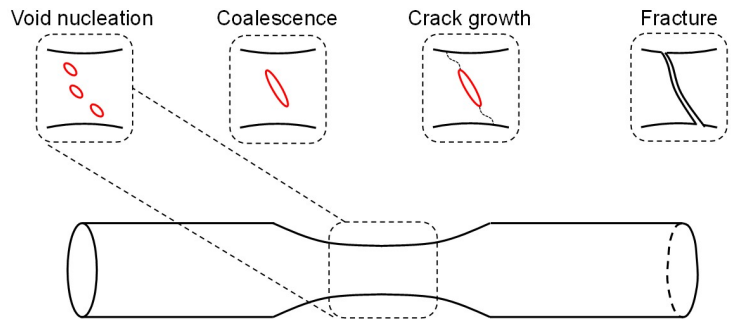

Figure 2.1: *Sequence of events in the progression of ductile fracture by nucleation and coalescence of voids followed by a micro-crack growth.*

2.1 Ductile damage and fracture modeling

The role of micro voids during the ductile fracture process was recognized early by McClintock [13] who attempted to correlate the radius of the nucleated cavities to the size of the plastic strain. During the same period Rice and Tracy [14] analyzed the evolution of spherical voids, compared to McClintock who assumed cylindrical voids, in a elastic-perfectly plastic material. In these early works on ductile fracture, the radius of the evolving cavity was assumed to be the governing aspect signaling failure when reaching a certain threshold value. Subsequently, the micro-mechanical modeling point of view on ductile fracture was introduced in the works by e.g. Gurson [15], Tvergaard [16] and Rousselier [17]. Here, a porosity term was introduced in the yield function, representing the void volume growth in the considered material. Needleman and Tvergaard [18] contributed to a further improvement of the work by Gurson, extending it to account for the acceleration in the failure process as a effect of void coalescence. Furthermore, in a later work by Pardoen and Hutchinson [19] the role on void spacing and void shape effects was addressed.

Even though these models are able to fairly well represent the physical phenomena on a micro-scale it is difficult to apply these concepts when considering large scale structures for the prediction of ductile fracture. Lemaitre [20], [11] aimed to bridge these scale levels by introducing an alternative continuum damage modeling framework on the intermediate macro-scale degrading the effective material via a scalar damage variable. In line with the introduction of the continuum damage approach to fracture, Johnson and Cook developed phenomenological models for the representation of the flow stress [21] and failure strain [22]. These models account for the effects of isotropic hardening, strain-rate, temperature and stress triaxiality. All important components in order to represent ductile fracture. However, it became quickly evident that it was difficult to capture the phenomena of strain localization, induced by strain softening in a mesh independent fashion. To remedy these issues, Bazant et al. [23], Bazant and Pijaudier-Cabot [24] elaborated on a non-local continuum damage approach. Subsequently, extensions to non-local micro-mechanical formulations were made by e.g. Tvergaard and Needleman [25] and Reusch et al. [26].

However, in situations when the crack paths are known á priori the cohesive zone concept, introduced by Dugdale [27] and Barenblatt [28] for elastic-plastic fracture in ductile materials, could be applied in a straight forward manner. In this modeling framework the degrading mechanisms in front of the crack tip are unified into a discrete line or plane, while a stress-displacement relation across the considered line or plane is used to represent the degradation in the fracture zone. Here, the separation (displacement jump) migth be achieved by applying interface elements and hence introducing regularized displacement discontinuities at the finite element (FE) interfaces see e.g. Larsson et al. [29]. However, an alternative approach is to embed the displacement jumps within the FE. To achieve this the standard displacement based FE approach needs to be enhanced with additional degrees of freedom, computed using a traction-separation law, to control the displacement jump see e.g. Ortiz et al. [30]. Needleman [31] used these concepts to describe the process of void nucleation from initial debonding through complete separation and subsequent void growth in ductile materials. Since the introduction of the cohesive zone framework, a vast amount of approaches for the representation of fracture has been conducted e.g. Ortiz and Pandolfi [32], Scheider [33], Remmers et al. [34]. The disadvantage of this approach is obvious when the crack path is unknown á priori, which leads to strong mesh dependence as evidenced by Scheider and Brocks [35]. During recent years the cohesive zone concept is often combined with the eXtended finite element methodology (XFEM) introduced by Belytschko and Black [36], who formulated the kinetics using the work by Melenk and Babuška on the concept of the partition of unity [37]. The XFEM was further improved by Moës et al. [38]. It is now often applied for the representation of mesh objective fracture response together with the cohesive zone framework e.g. Zi and Belytschko [39], Larsson [40] and Fagerström [41]. In addition, XFEM is nowadays also combined with computational homogenization, where multi-scale modeling on a micro- and macro scale level is used to represent the ductile fracture process e.g. Svenning [42].
Recent developments on diffuse crack models based on the introduction of a crack phase-field for the representation of the the sharp crack discontinuity by Miehe et al. [43], [44] have been adopted frequently, see Figure 2.2. This approach models the transition from crack nucleation to propagation, representing both the merging and branching of cracks

in a natural fashion. Developments to represent the transition from brittle to ductile fracture have been made by Miehe et al. [45] and pure ductile fracture by Ambati et al. [46].

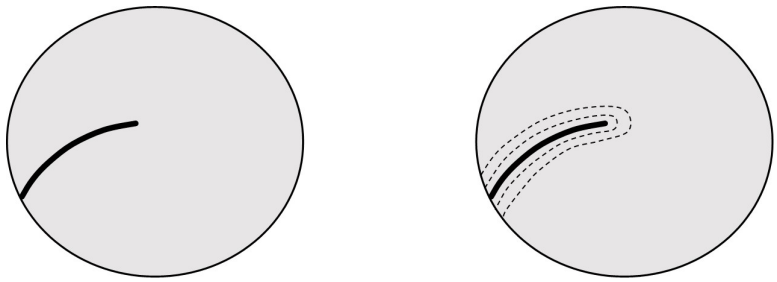

Figure 2.2: *Left) A sharp crack within a solid. Right) Representation of the regularized diffuse crack surface.*

2.2 The machining process - orthogonal cutting

Damage and fracture are also manifested during machining processes. It is primarily related to the removal of material from the workpiece to achieve appropriate dimensions within reasonable tolerances. However, to model the the machining process and increase the understanding of the material behavior, including the complex phenomena occurring at the vicinity of the cutting tool it is important to have an understanding of the general mechanisms during the process.

2.2.1 The material flow

Let's consider Figure 2.3 which illustrate the orthogonal machining process (2D turning), where the cutting tool is perpendicular to the direction of motion of the workpiece. During this process a material portion called "*chip*" is removed from the workpiece under the occurrence of a diversity of physical phenomena e.g. large elasto-plastic deformations, high strain-rates, thermo-mechanical coupling, complicated contact conditions and chip separation. The major deformation during the machining process, which occurs at the vicinity of the cutting tool, is concentrated within three different zones; the *primary*, *secondary* and *tertiary* deformation zones as illustrated in Figure 2.3.

To increase the productivity and efficiency of the machining process and hence meet the escalating customer demands an increase in material removal rate e.g. cutting speed, feed rate and depth of cut is most often the solution. However, the increasing material removal rates results from the high deformation rates involved in these processes which lead to a severe shear localized deformation in the *primary* deformation zone. This leads to a high temperature increase in this region which is a consequence of the large amount of heat generated due to energy dissipation from the highly localized plastic deformation in the vicinity of the cutting tool edge.

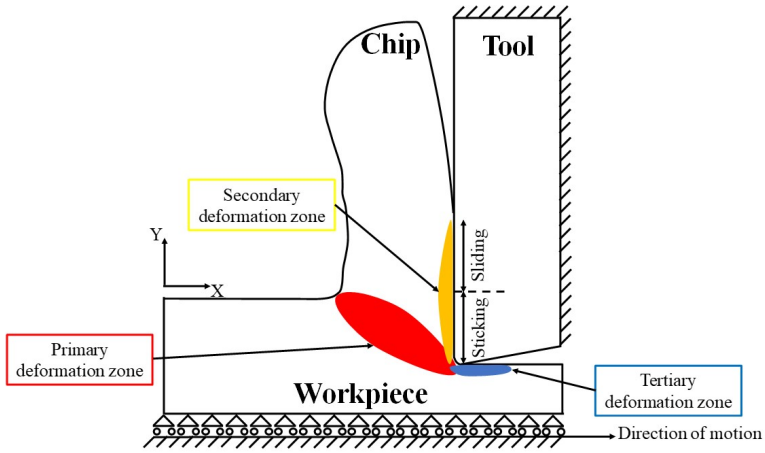

Figure 2.3: *Illustration of the primary, secondary and tertiary deformation zones during orthogonal cutting.*

However, in the *secondary* deformation zone complex contact conditions occur between the inner surface of the chip and the tool surface. Briefly, this zone can be separated into two distinct regions as illustrated in Figure 2.3 namely, the *sticking* and *sliding* region, respectively. Due to the high contact pressure at the cutting tool edge, the chip material might stick to the tool surface hence refereed to as the sticking region. With an increasing distance from the cutting tool edge, the contact pressure along the rake face successively decreases leading to a sliding of the chip material against the tool surface. As the plastic deformations along this zone are shown to be larger than in the primary deformation zone and the occurrence of friction at the contact, a significantly higher temperature increase might be observed compared to the primary deformation zone. Consequently, the high pressure and temperature in this zone lead to high thermo-mechanical loads which are primarily responsible for the tool wear [47].

As material is removed from the workpiece new surfaces are created in the *tertiary* deformation zone in Figure 2.3. Here, the sliding of the tool edge along these surfaces can induce deformations in this region. This will, influence the material and component properties e.g. residual stresses, surface roughness and microstructural phase transformations in this region.

2.2.2 Chip formation

Depending on the workpiece material considered and cutting conditions applied, the chip morphology might vary. Machining a ductile material at low cutting speeds often results in the formation of *continuous* chips. However, if the chip breakage is poor it is most likely that too long chips will form especially at low cutting speeds. This will successively lead to the adhering of the workpiece material to the tool surface due to pressure welding hence creating the formation of the *chip with a built-up edge*. When machining e.g. titanium alloys and nickel-based superalloys at relatively high cutting

speed a *shear-localized* chip formation is manifested. The occurrence of this type of chips is often explained by the onset of instability due to the adiabatic shear band formation in narrow, highly deformed, regions [48], [49]. Yet another explanation for the development of this type of chip is the crack/damage initiation and subsequent propagation [50], [51]. Finally, if a naturally brittle material is considered e.g. Gray Iron or Compacted Graphite Iron (CGI) a *discontinuous* chip formation is often observed [52]. Note though it was found in **Paper C** that the inelasticity of CGI should be considered.

2.2.3 Cutting forces

During the machining (turning) operation as seen in Figure 2.4, the cutting tool is subjected to different forces at the vicinity of the cutting edge. These forces affect the performance of the tool e.g. wear, the product quality, the machine power needed and the dynamics of the system among others. Figure 2.4 illustrates the forces acting on a 3D tool edge. The *cutting* force F_c acts in the cutting direction. The *feed* force F_f acts tangentially to the cutting force. Hence, it is parallel to the feed direction while the *passive* force F_p is acting perpendicular to the feed force.

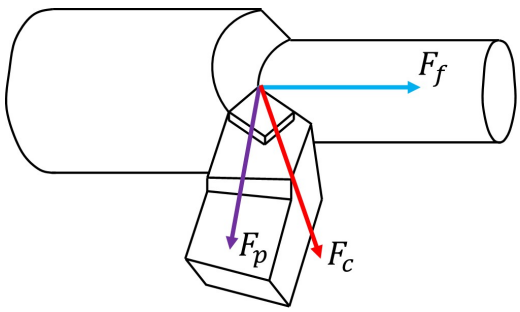

Figure 2.4: *Illustration of the forces acting on the cutting tool during 3D turning operation.*

2.2.4 Modeling approaches

In the mid 20^{th} century, the machining process was modelled using *analytical models* which at this stage of the development described the basic mechanics behind machining e.g. orthogonal cutting by means of simplified assumptions on the cutting zone. Here the pioneering work by Merchant [53] and Oxley [54] are among the central and most important works at the time. These works are still used for calibration purposes of the flow stress response e.g. Malakizadi et. al. [55]. However, with the successive increase in computer power and the introduction of the FEM, the *numerical modeling* of the machining process gained scientific interest during the 1970s. Among the first to apply the FEM to model the machining process was Shirakasi and Usui [56]. Since then a set of numerical modeling strategies have been developed with respect to the FEM, primarily with respect to the Lagrangian and Eulerian methods.

In the Lagrangian method the FE mesh is interlaced with the material motion while

in the Eulerian approach the mesh is fixed in space allowing the material to flow through. Both approaches have their advantages and disadvantages. For instance, applying the Lagrangian method to machining simulations often results in an extensive distortion of the elements if not e.g. a re-meshing technique is adopted [5], [57]. However, it allows for the simulation of the chip formation without knowing the morphology á priori which is a must when the Eulerian method is considered. To avoid the frequent re-meshing with respect to the Lagrangian method the Arbitrary-Lagrangian-Eulerian method has been developed and applied to the modeling of machining [58], [59], [60]. This method combines the best features of the Lagrangian and Eulerian methods.

2.2.5 Constitutive and fracture modeling

Machining is a rapid material removal process during which high cutting speeds often result in large strains, high strain-rates and elevated temperature which affects the material response, see section 2.2.1. Evidently, these complex phenomena (among others) have been extensively investigated experimentally in order to increase the knowledge and understanding of the chip formation process and the activation of different microstructural mechanisms. With increased understanding of the fundamental mechanisms the development of more accurate, efficient and robust processes has been achieved. To further accelerate the accumulation of knowledge within the field, numerous of numerical models have been developed. These models strive to explain, capture and predict not only chip formations but as well tool wear and the evolution of damage during the machining process. Therefore, to increase the reliability of the numerical models accurate constitutive models are considered to be highly necessary for the representation of the workpiece material behavior under machining conditions. For this purpose, there exist phenomenological models for the representation of the flow stress response e.g. the Johnson-Cook constitutive model [21] and modified versions of the model [61]. The Zerilli-Armstrong constitutive model [62] is a dislocation-mechanics-based constitutive model relating the effects of strain, strain-rate and temperature to the activation of dislocations. Another model is the extended modified Bai-Wierzbicki model [63], which accounts for the influence of the state of stress, strain-rate, temperature and damage on the flow stress response. Depending on the heat treatment of the workpiece material e.g. machining hardened steel, constitutive models accounting for the effect of hardness are developed and proposed by Umbrello et al. [64]. The methodology of physically based constitutive models, where the knowledge of the underlying softening and hardening mechanisms are central ingredients for the representation of the material response is developing fast e.g. [65],[66], [67]. However, it requires a significant amount of parameters to be calibrated.

On the other hand, the creation of new surfaces or rather separation of material that occurs during machining needs to be modelled and hence, different approaches are possible. For instance a predefined line in front of the tool tip can be assigned for the fracturing in relation to a separation criterion. The separation criterion can be defined either by a geometrical or physical relation. In the work by Shirakasi and Usui [56], the geometrical relation concern the distance the tool has penetrated into the FE discretized workpiece was considered. However, the physical criterion for the signaling of the separation along the predefined line are based on tensile plastic work [68], strain energy density [69] among

others. The material separation can also be achieved without assigning any predefined line in the workpiece material. This is represented by considering the plastic deformation hence modeling the chip formation process as a forming process which unfortunately leads to excessive distortion of the elements if not e.g. adaptive re-meshing is applied. However, modifying existing phenomenological constitutive models to incorporate strain softening effects has been shown to be yet another possible modeling technique where there is no need for any fracture criterion for the material separation as re-meshing is considered e.g. [61], [70]. Yet another approach is to consider the continuum damage modeling framework for the creation of surfaces. In this approach the effective material is enhanced with a fracture criterion e.g. based on fracture strain [22], hydrostatic influence [68] to mention some alternatives. This approach, combining a phenomenological constitutive model with an appropriate fracture criterion is an often adopted strategy e.g. [71], [72]. Whenever the criterion is reached damage evolution occurs. Recently, the implementation of non-local modeling approaches within the machining community have gained interest [73], [74].

3 Continuum damage and ductile fracture modeling

The objective with this chapter is, to describe the modeling framework developed for the ductile material and fracture process. To represent the ductile fracture process, a damage enhanced continuum of Lemaitre type is considered where the effective material is coupled to a damage evolution law. Here the damage evolution is promoted by a damage driving energy, consisting of elastic and inelastic contributions. To account for a flexible ductile fracture modeling, a damage threshold criterion is introduced. Whenever the criterion is fulfilled the inelastic damage driving energy is initiated thus leading to a substantial evolution of damage and, a progressive loss of material integrity. On the one hand, the local character of the adopted modeling framework contributes to computational efficiency and robustness, while on the other results in an induced mesh dependence. To overcome the issue, an mesh objective enhancement of the continuum damage modeling is proposed in order to strengthen the modeling approach.

3.1 Pre- and post localization response

Ductile fracture is often associated with considerable amount of plastic deformation á prior to fracture. Considering a circular notched specimen subjected to tensile loading as in Figure 3.1, a "*necking*" or *localization* region will occur in the notch after continuous deformation.

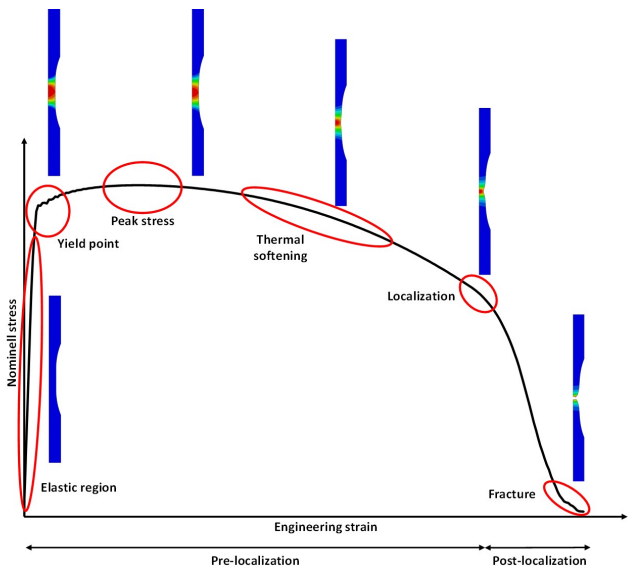

Figure 3.1: *The material response for a ductile material illustrating the pre- and post localization regions.*

Subsequently, formation of voids and micro-cracks occur and coalesce on a micro-structural level to form macroscopic cracks induced by shear deformation, and hence eventually leading to a compete fracture. Moreover, as the process is slow, it allows for the absorption of large amount of energy in the material. To describe the response of deforming ductile materials in more detail, it can be divided in to two predominant regions the *pre-* and *post* localization regions as shown in Figure 3.1.

The *pre-localization* response can be split into two parts. Firstly, an elastic response is manifested where the induced deformation due to the loading is reversible. This implies that, the material response is completely recovered to its initial state upon unloading. Secondly, if a continuous loading is carried out beyond the yield point, the material enters a irreversible state, where there will always remain a permanent plastic deformation after unloading. Upon further loading the plastic deformation become significant, which is reflected by an local increase in temperature in those regions. This leads to a successive thermal softening of the material, and a subsequent localization in narrow bands hence, formation of the "*necking*". Along these bands the material successively lose its load carrying capacity (integrity) and hence, enters the *post- localization* regime.

Besides, an increase in thermal softening, a damage initiation and propagation followed by a complete fracture is often manifested during the *post- localization* response. Here voids and micro-cracks are assumed to be formed, resulting in a initiation of damage. The propagation of the damage is governed by the growth of these voids and micro-cracks to eventually coalesce into macro-cracks leading to a complete fracture. Therefore, it is highly important to be able to capture these phenomena in order to properly describe the material response and degradation in this regime.

To represent the continuum response during the deformation and fracturing process, an appropriate formulation of the effective material combined with a damage evolution law is developed. The modeling framework should, in addition, account for the important occurring phenomena during the process e.g. strain hardening, strain-rate and thermal softening in order to accurately predict the material behavior.

3.2 Damage enhanced effective material

The modeling framework for the representation of ductile fracture developed in this work is intended to be put in the context of modeling and simulation of machining processes. Therefore, it is of significant interest that the effective material response is formulated so that it captures and accounts for the thermal softening during the deformation. As machining is a rapid process, the effect of strain-rate and material hardening needs to be additionally captured. Besides the material behavior, the separation of material or fracturing process needs to be modelled. As pointed out in section 3.1, the crack/damage propagation in a ductile material is promoted by shear deformation. In fact, shear deformation is the predominant deformation mode occurring in the primary deformation zone during machining. Therefore, damage evolution should primarily be promoted by shear deformation to represent the deformation and fracturing during machining.

For this purpose, a scalar damage enhanced visco-plastic effective material model is formulated in **Paper A** and **Paper B** to represent the progressive loss of material integrity

during the deformation process. To promote damage evolution by shear deformation, the isochoric part of the effective material is degraded by the degradation function $f[\alpha]$ in **Paper B**, compared to **Paper A** where the complete effective material response is degraded, as

$$\psi = f[\alpha]\rho_0\left(\hat{\psi}^{iso}[\bar{\boldsymbol{b}}] + g[\theta]\hat{\psi}^{mic}[k]\right) + \rho_0\hat{\psi}^{vol}[\bar{J},\theta] + \rho_0\hat{\psi}^{th}[\theta] \tag{3.1}$$

here $\hat{\bullet}$ denotes quantities of the effective material while $\bar{\bullet}$ represent reversible quantities. Moreover, $\hat{\psi}^{iso}$ is the isochoric part of the free energy, $\hat{\psi}^{mic}$ represents the stored free energy due to internal hardening processes in the material, $\hat{\psi}^{vol}$ is the stored free energy due to volumetric deformation and $\hat{\psi}^{th}$ is the stored free energy induced by the temperature. Additionally, ρ_0 corresponds to the density in the reference configuration, α is the scalar damage variable, $\bar{\boldsymbol{b}}$ is the reversible Finger tensor, θ is the temperature while k represents the inelastic straining and $\bar{J}$ denotes the reversible volumetric deformation. Finally, $g[\theta]$ is the temperature degradation function accounting for the induced thermal softening in the effective material as

$$g[\theta] = \begin{cases} 1 & \theta \leq \theta_{room} \\ 1 - \left(\frac{\theta - \theta_{room}}{\theta_{melt} - \theta_{room}}\right)^m & \theta_{room} < \theta < \theta_{melt} \\ 0 & \theta \geq \theta_{melt} \end{cases} \tag{3.2}$$

where m is an exponent of the temperature degradation, θ_{room} and θ_{melt} are room and melting temperatures, respectively.

It should be highlighted that the Johnson-Cook (JC) constitutive model [21] is applied as the prototype for the representation of the flow stress and thus indirectly the effective material response in **Paper A** - **Paper D** and is defined as

$$\hat{\tau}_y = \left(A + Bk^n\right)\left(1 + C\log\left[\frac{\dot{k}}{\dot{\epsilon}_0}\right]\right)g[\theta] \quad \text{for} \quad \dot{k} \geq \dot{\epsilon}_0 \tag{3.3}$$

This relates to the fact that is often considered for the modeling and simulation of machining as it accounts for the effects of isotropic hardening via the yield stress A, hardening stress B and the hardening exponent n. Further, the influence of strain-rate is via the viscosity parameter C, the reference strain rate $\dot{\epsilon}_0$, the inelastic strain rate $\dot{k}$ and thermal softening is via the degradation function $g[\theta]$. It is worth noting that in **Paper A** and **Paper C** the strain-rate dependence and thermal softening effects in the JC constitutive model were neglected hence, quasi-static and iso-thermal conditions were assumed to prevail.

To obtain the proper thermodynamic coupling the proposed damage enhanced effective material framework in **Paper B** is based on continuum thermodynamics, whereby the dissipated energy respects the first and second law of thermodynamics, respectively. As machining is a rapid process, it might be assumed that the temperature in the primary deformation zone does not have sufficient time to dissipate and thus adiabatic conditions can be assumed to prevail together with the non-existence of a heat source. Hence, the

total mechanical dissipation is formulated consisting of a degraded effective part $\hat{\mathcal{D}}$, the elastic $\mathcal{A}$ and inelastic $\mathcal{B}$ damage driving parts as

$$\begin{aligned} &\mathcal{D} = f[\alpha]\hat{\mathcal{D}} + \mathcal{A}\dot{\alpha} = \dot{\overline{f[\alpha]\hat{\mathcal{D}}_T}} + (\mathcal{A}+\mathcal{B})\,\dot{\alpha} \geq 0 \\ &\text{with} \quad \hat{\mathcal{D}} = \hat{\boldsymbol{\tau}}^{\text{iso}} : \boldsymbol{d}_p + \hat{\kappa}\dot{k} \geq 0 \quad \text{and} \quad \mathcal{B} = -f'[\alpha]\hat{\mathcal{D}}_T \geq 0 \end{aligned} \tag{3.4}$$

where $\hat{\mathcal{D}}_T = \int_0^t \hat{\mathcal{D}}\, dt$ is the total effective dissipation, $\dot{\alpha}$ is the rate of damage, $\hat{\boldsymbol{\tau}}^{iso}$ is the isochoric Kirchhoff stress tensor, $\hat{\kappa}$ is the micro hardening stress and $\boldsymbol{d}_p$ is the plastic rate of deformation tensor. In line with the limitations on the thermodynamics e.g. adiabatic conditions, a simplified version of the energy equation is formulated as

$$c_v\dot{\theta} = w^p + \mathcal{A}\dot{\alpha} - 3K\alpha_\theta\theta\mathbf{1} : \boldsymbol{d} - f[\alpha]\left(\hat{\kappa} + \theta\frac{\partial\hat{\kappa}}{\partial\theta}\right)\lambda \tag{3.5}$$

where c_v is the specific heat capacity, w_p is the plastic work, $3K\alpha_\theta\theta$ is the thermal stress, $\boldsymbol{d}$ is the full rate of deformation tensor while λ is the plastic multiplier. From Eq.(3.5) it could be observed that the elastic damage contributes to the heat generation, while the thermal stress and micro hardening require a portion of the energy to develop. This, leads to a slight temperature decrease upon initial loading due to cold work.

3.3 The onset of inelastic damage driving energy

Key features for the representation of the ductile fracture response concern the introduction of the *total damage driving energy* in connection to a damage threshold criterion in **Paper A** and **Paper B**. Moreover, the damage threshold criterion acts as a barrier to be surpassed before the accumulation of the inelastic damage driving energy is initiated at time $t \geq t_f$, where t_f is the damage threshold time. To arrive at a expression for the *total damage driving energy*, it is assumed that the inelastic damage driving energy $\mathcal{B}$ in Eq.(3.4) could be subdivided in a initial $\mathcal{B}^i$ and fracture $\mathcal{B}^f$ portion which are separated by the damage threshold time $t = t_f$. Thus, from the resulting thermo-mechanically motivated dissipation rate in Eq.(3.4) and using that $\dot{\overline{f[\alpha]\hat{\mathcal{D}}_T}} = \dot{\overline{f[\alpha]\hat{\mathcal{D}}_T^f}} - \mathcal{B}^i\dot{\alpha}$ for $t \geq t_f$, the total mechanical dissipation during the entire loading process presented in **Paper B** can be expressed as,

$$\mathcal{D}[t] = \begin{cases} f[\alpha]\,\hat{\mathcal{D}} + \mathcal{A}\dot{\alpha} & 0 \leq t \leq t_f \\ \dot{\overline{f[\alpha]\hat{\mathcal{D}}_T^f}} + \left(\mathcal{A}+\mathcal{B}^f\right)\dot{\alpha} & t \geq t_f \end{cases} \tag{3.6}$$

where $\hat{\mathcal{D}}_T^f$ is the accumulated effective dissipation $\hat{\mathcal{D}}$ from time $t \geq t_f$. Evidently, in the formulation of the mechanical dissipation, the *total damage driving energy*, $\mathcal{A}_T$, consists of different contributions before and after the damage threshold criterion is reached at time $t = t_f$. This might be expressed as,

$$\mathcal{A}_T = \begin{cases} \mathcal{A} = -f'[\alpha]\hat{\psi}^{iso} & 0 \leq t \leq t_f \\ \mathcal{A}+\mathcal{B}^f = -f'[\alpha]\left(\hat{\psi}^{iso} + \hat{\mathcal{D}}_T^f\right) & t > t_f \end{cases} \tag{3.7}$$

Note, the major difference regarding the onset of damage evolution, between the formulations in **Paper A** and **Paper B**, relate to the accumulation and release of the parts related to the *total damage driving energy*. In **Paper A**, the release of the elastic and accumulation of the inelastic contributions occur when the damage threshold criterion is signaled.

To model the ductile fracture behavior, it is of significant interest that the damage threshold criterion is physically motivated. For this purpose, the JC failure model [22], derived and developed for the representation of ductile fracture, is applied in **Paper A**–**Paper C**. This model accounts for the influence of stress triaxiality via d_2 and d_3, strain-rate through d_4 and thermal softening via d_5 for the prediction of the failure strain ϵ_f which is formulated as,

$$\epsilon_f = \left(d_1 + d_2 \exp\left[d_3 \frac{\hat{p}}{\hat{\tau}_e}\right]\right)\left(1 + d_4 \log\left[\frac{\lambda}{\dot{\epsilon}_0}\right]\right)\left(1 + d_5 \frac{\theta - \theta_{room}}{\theta_{melt} - \theta_{room}}\right) \tag{3.8}$$

Here d_1 relates to the amount of plastic deformation that is required to initiate the onset of damage evolution while $\hat{p}$ and $\hat{\tau}_e$ corresponds to the effective pressure and the effective von Mises stress, respectively. Basically, when the accumulated plastic strain reaches the computed failure strain at time $t = t_f$ the damage onset threshold is signaled. Another often used criterion is the one based on the accumulated plastic work developed by Cockcroft and Latham [68]. A modified version of the Cockcroft and Latham criterion is developed in **Paper D** which accounts for the effect of stress triaxiality as it has been shown to be important for the modeling and simulation of machining by e.g. Lorentzon et al. [75].

3.4 The damage evolution

The considered continuum damage point of view on the modeling, results in a pathological mesh dependence. This phenomena is manifested through the decrease in the numerical displacement (strain) to failure and an localization of the strain in narrow bands with an refined FE discretization, seen in Figure 3.2 for a square plate loaded in shear. To overcome the pathological mesh dependence, a mesh objective enhanced *smeared damage* model is purposed for the representation of the damage evolution in **Paper A**. Meanwhile, in **Paper B**, a *continuum damage* modeling approach derived based on continuum thermodynamics is considered. Thus, in general, both modeling approaches are developed within the continuum damage framework where concepts from the phase field modeling are combined with the principle of maximum dissipation.

3.4.1 Smeared damage modeling approach

In **Paper A** the smeared damage modeling approach was applied for two significantly different damage evolution laws. The first represent the augmented *element removal model* while the second is an in-house developed *progressive damage model*. The difference between the models considering the stress-strain response (for one finite element) under tensile and compressive loading can be seen in Figure 3.3. An instantaneous stress drop of

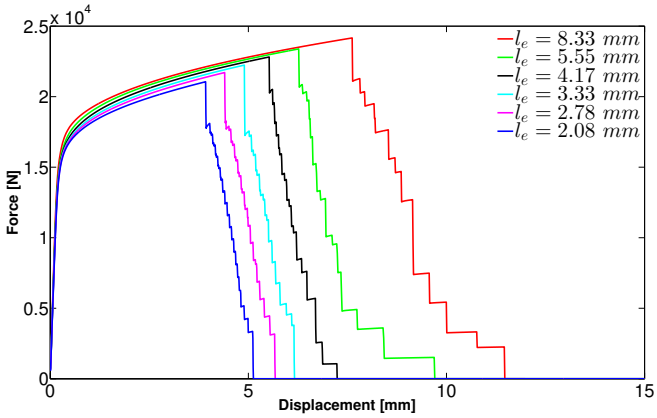

Figure 3.2: *Pathological mesh dependence using the Johnson-Cook failure model to represent ductile fracture for varying FE discretizations, where l_e is the element length.*

all stress components is obtained whenever damage evolution is signaled when considering the element removal model. In contrast to this model, a smooth degradation of the stress is manifested for the progressive damage evolution model.

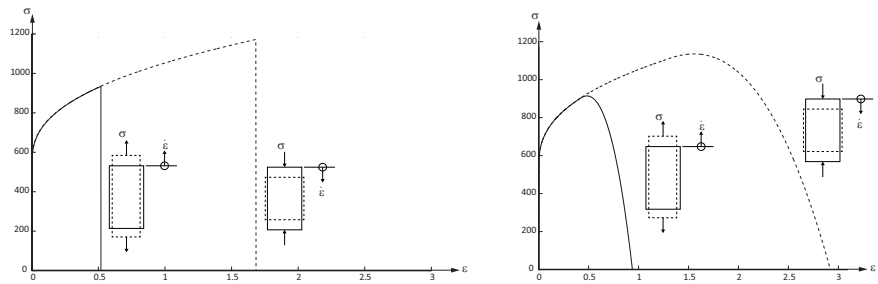

Figure 3.3: *Stress response in uniaxial compression and tension for the two considered damage models from* **Paper A** *in a single element: Left) The element removal model and Right) The progressive damage model.*

The governing idea for these ductile damage models is based on the relation between the continuum dissipation per unit volume during the fracture process and the fracture dissipation rate due to crack surface propagation. The former is defined via the dissipation potential G due to the diffuse crack surface propagation, from the phase-field context [45], and formulated as,

$$G = \int_{\mathcal{B}_0} \mathcal{G}_c \gamma[\alpha]\, dV \quad \text{where} \quad \dot{G} = \int_{\mathcal{B}_0} \mathcal{G}_c \frac{\partial \gamma}{\partial \alpha} \dot{\alpha}\, dV \geq 0 \tag{3.9}$$

where $\mathcal{G}_c$ is the fracture energy release rate while the γ- field corresponds to the diffuse

fracture area density. To arrive at a mesh objective smeared damage formulation it is assumed that the damage field is "localized", meaning that the damage variable α is confined within one element width in the FE application as illustrated in Figure 3.4.

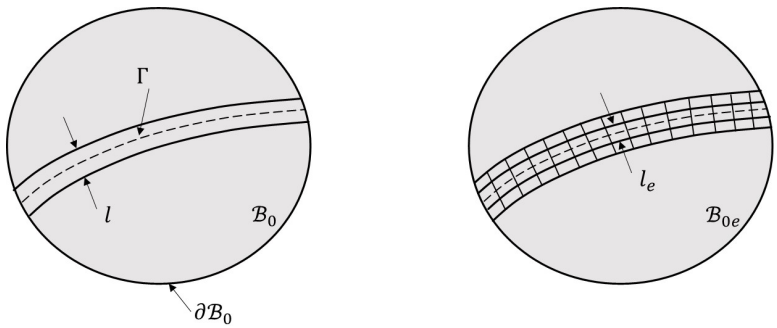

Figure 3.4: *Left) A solid $\mathcal{B}_0$ with an assumed localized distribution of the damage field along fracture surface Γ. Right) FE discretization of the solid, where the element size l_e determines the width of the localized zone l.*

As the damage field, obtained from the solution to the momentum balance and the constitutive equations, is assumed to be "localized" the dissipation for different FE discretizations should be consistent with respect to a reference (representative) FE discretization. Typically, the reference FE discretization l_r is obtained when the numerical solution is considered converged. This provides a possibility to increase the computational efficiency for the FE simulations by applying coarser FE discretizations l_e while still obtaining an accurate solution for the numerical problem.

Hence, the conservation of the fracture dissipation energy is obtained by ensuring that the continuum dissipation rate during the fracture process, at time $t \geq t_f$, is converted to the fracture dissipation rate, which can be defined as

$$\int_{\mathcal{B}_0} \mathcal{G}_c \frac{\partial \gamma}{\partial t}\, dV = \int_{\mathcal{B}_0} \mathcal{D}_\alpha\, dV \tag{3.10}$$

where $\mathcal{D}_\alpha$ is the constrained maximum of the continuum fracture dissipation rate defined as

$$\mathcal{D}_\alpha = \max_{\mathcal{A}_T,\, \mu} \; f[\alpha]\hat{\mathcal{D}} + \mathcal{A}\dot{\alpha} - \mu\phi_\alpha \geq 0 \tag{3.11}$$

Now, to formulate the damage evolution law for the *element removal* model and the *progressive* damage model developed in **Paper A** two significantly different evolution laws are proposed for respective model,

$$\dot{\alpha} = \mu \frac{\partial \phi_\alpha}{\partial \mathcal{A}_T} \mathcal{H}_S[t - t_f] \quad \text{and} \quad \dot{\alpha} = \delta_S[t - t_f] \tag{3.12}$$

Here the first expression corresponds to the *progressive* damage evolution law where the Heaviside function $\mathcal{H}_S[t-t_f]$ ensures that the damage evolution will not commence until the damage threshold is signaled at time $t = t_f$. Furthermore, the second formulation represent

the instantaneous damage evolution law for the *element removal* model. Whenever the dirac-delta function $\delta_S[t - t_f]$ is signaled a damage evolution is manifested. To control the damage evolution, a damage loading function is introduced as

$$\phi_\alpha = \mathcal{A}_T - g[\alpha] \leq 0 \tag{3.13}$$

where $g[\alpha]$ is a damage function that controls the progression of the damage evolution after damage threshold criteria has been reached and vary between the considered damage laws e.g. $g[\alpha] = \mathcal{A}_c(1 + c\alpha)^{m_d}$ for the *progressive* damage model.

Merging these concepts lead to a scaling factor for respective damage evolution law. The scaling factor secures that the same amount of dissipated energy, as for a reference FE discretization l_r, is released during the fracture process when other FE discretizations l_e are considered. Basically, the factors are used to scale the *total damage driving energy* $\mathcal{A}_T$ and are defined as

$$c[l_e] = \frac{l_r}{l_e}\Big(c_r + m_d + 1\Big)\Big(m_d + 1\Big) \quad \text{and} \quad l_e\mathcal{A}_T = \mathcal{G}_c = \mathcal{A}_c l_r \tag{3.14}$$

Here m_d is a exponent controlling the damage evolution rate and defined in $g[\alpha]$ for the *progressive* damage model. The damage evolution parameter c_r is assumed to be defined based on a representative FE discretization l_r. For the element removal model, the damage driving energy $\mathcal{A}_T$ is scaled with respect to the $\mathcal{A}_c = \mathcal{A}_{t=t_f}$ which is the elastic damage driving energy to be released as if an instantaneous damage evolution would have occurred at time $t = t_f$.

3.4.2 Concluding results - Smeared damage approach

In **Paper A** it is shown that the mesh objective enhancement is able to remove the mesh dependence seen in Figures 3.5 - 3.6, when quasi-static and iso-thermal conditions are considered. One may note the difference between results in Figure 3.2 and 3.5, in Figure 3.5 there is a clear convergence when l_e decreases.
However, when a relatively fine representative FE discretization l_r is chosen the *element removal* model fails to scale the damage driving energy for coarser FE discretizations thus, leading to a overestimation in peak force and displacement at failure. This is primarily related to the release of elastic damage driving energy $\mathcal{A}_c = \mathcal{A}_{t=t_f}$ which evidently becomes too large when coarser FE discretizations are used. As a matter of fact, the scaling is implemented when the damage threshold criterion is signaled, which is based on the fracture strain computed by the JC fracture criterion. So, for coarser FE discretizations a larger fracture strain is predicted, leading to an overestimation of the elastic damage driving energy. On the other hand, the progressive damage model is able to scale both coarser and finer FE discretizations resulting in a mesh objective response.

The mesh objective simulated results originate from a numerical shear problem (a square plate loaded in shear) where the damage pattern is always localized within one element width and where a structured FE discretiztion is considered. However, if a unstructured FE discretization is considered for the numerical shear problem of a hat specimen in [76], the damage models are shown to be able to capture representative

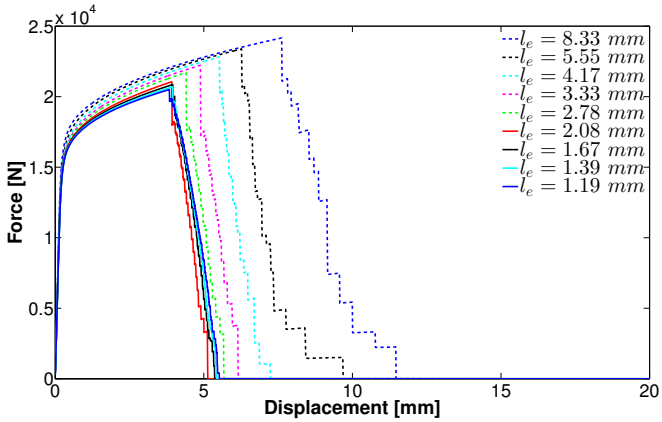

Figure 3.5: *force versus displacement response for the element removal model with mesh objective regularization where the reference element length* $l_r = 50/24$ *mm.*

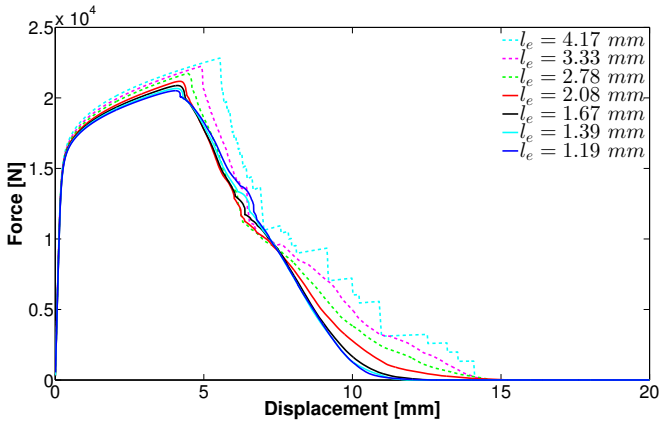

Figure 3.6: *force versus displacement response for the progressive damage model with mesh objective regularization where* $l_r = 50/24$ *mm,* $c_r = 2$*,* $m_d = 1$*.*

damage modes. In this case, the damage patterns do not localize within one element width which result in a mesh dependence. Quantitatively, however, a good agreement is obtained for the effective stress and plastic strain levels.

With the models in **Paper A**, the damage driving energy is still based on a numerical representation without any correlation to the actual fracture energy for the considered material. Hence, besides the use of the JC models the approach lacks a complete physical representation of the ductile damage and fracture process. Therefore, to better model this process it is beneficial if the considered damage model is able to reflect the characteristics of ductile fracture e.g. void nucleation and growth. In addition, the effect of thermal softening and strain-rate are important in order to simulate the machining process.

3.4.3 Continuum damage modeling approach

In **Paper B** the modeling of the ductile damage and fracture process is placed in the context of continuum damage and fracture modeling where a progressive damage law, leading to a physically motivated damage evolution, is proposed.

Following the similar line as in section 3.4.1, the damage field is assumed to be localized around the fracture surface Γ_s surrounded by a diffuse damage in the neighboring region as seen in Figure 3.7.

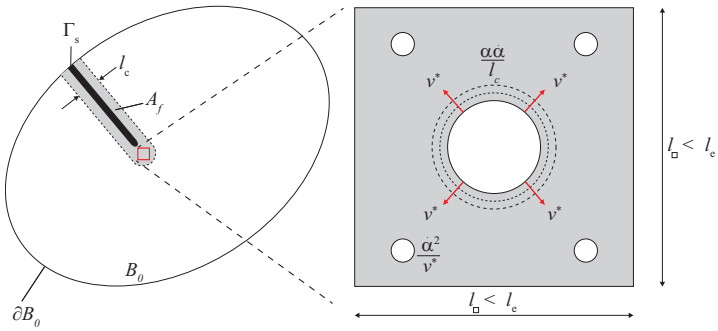

Figure 3.7: *Interpretation of damage area progression in terms of void growth for existing and nucleated voids in the localization zone. Note that $l_\square$ represent a portion of the localized damage width l_c.*

To represent the diffuse character of the damage around the fracture surface, the diffuse fracture area functional A_f is considered. This functional is made up of the diffuse fracture area density $\gamma[\alpha, \dot{\alpha}]$ as in section 3.4.1 and formulated as,

$$A_f = \int_{\mathcal{B}_0} \gamma \, d\mathcal{B} \quad \text{with} \quad \gamma = \int_0^\alpha \left(\frac{\alpha}{l_c} + \frac{\dot{\alpha}}{v^*} \right) d\alpha \tag{3.15}$$

where the diffuse fracture area density is characterized by the finite fracture area progression speed v^*, the rate of damage $\dot{\alpha}$ and the internal length parameter l_c assumed to represent the width of the diffuse fracture area. To arrive at a progressive damage model for the representation of ductile damage and fracture, the dissipation potential in Eq.(3.9) is considered. Via this the potential, it is possible to establish a global balance relation between the *produced* energy dissipation and the *input* damage dissipation rate. Here, the fracture area progression rate $\dot{\gamma}$ and the fracture dissipation due to the damage driving energy in Eq.(3.6) is assumed to promote the *produced* and *input* contributions, respectively. In summary, this is formulated as,

$$\dot{G} = \underbrace{\mathcal{G}_c \int_{\mathcal{B}_0} \dot{\gamma} \, d\mathcal{B}}_{produced} = \underbrace{\int_{\mathcal{B}_0} \mathcal{A}_T \dot{\alpha} \, d\mathcal{B}}_{input} \tag{3.16}$$

To represent the fracture area progression, the rate $\dot{\gamma}$ with respect to the ductile damage

and fracture response is formulated as,

$$\dot{\gamma} = \frac{1}{l_c}\alpha\dot{\alpha} + \frac{1}{v^*}\dot{\alpha}^2 \geq 0 \tag{3.17}$$

which corresponds to a convective term $\frac{1}{l_c}\alpha\dot{\alpha}$ and a local damage production term $\frac{1}{v^*}\dot{\alpha}^2$. These terms could be assumed to represent the growth of existing voids and void nucleation in the diffuse fracture region as illustrated in Figure 3.7.

Now by combining a similar damage loading function as in Eq.(3.13) and using constraint maximum of the damage driving part of the total dissipation rate in Eq.(3.6) the progressive damage evolution law is obtained as

$$l_c\dot{\alpha} = v^* < \alpha^s[\alpha] - \alpha > \quad \text{with} \quad \alpha^s = \frac{\mathcal{A}_T[\alpha]l_c}{\mathcal{G}_c} \tag{3.18}$$

where $< \bullet >$ is the positive part function (or Macaulay brackets) and α^s corresponds to the source due to elasto-plastic damage driving energy. It is worth mentioning that as $v^* \to \infty$ the whole damage evolution is controlled by the elasto-plastic deformation. However, the fracture area progression speed v^* eventually converges towards a finite speed. Applying a lower or much lower v^* than the converged results in a increased material ductility due to the fact that the local damage production $l_c\dot{\alpha}$ in Eq.(3.18) has time to develop and hence the damage evolution rate decreases.

3.4.4 Concluding results - Continuum damage approach

The progressive damage model was validated against a preheated cylindrical test specimen subjected tensile loading at high strain-rates from [77]. The effect of the elastic and inelastic contributions of the total damage driving energy $\mathcal{A}_T$ at the initial temperatures 100 °C, 300 °C and 500 °C is illustrated in Figure 3.8a and compared with experimental force versus displacement curves from [77]. The results show that the proposed modeling framework is able to predict the force versus displacement response in good agreement with experiments for temperatures up to 300 °C. The influence of the elastic damage driving energy is overall insignificant compared with the inelastic contribution and decreasing with increasing initial temperature. Additionally, a good mesh convergence is obtained, as seen in Figure 3.8b, for the preheated 300 °C test specimen. The convergence is preserved until the final stage of the loading where a damage mode shift occur for the finest FE discretization and is most likely a explanation for the reduced mesh convergence in this stage as discussed in **Paper B**.

Figure 3.9 illustrates the effect of the void nucleation term $\frac{1}{v^*}\dot{\alpha}^2$ compared to the static damage evolution $\alpha = \alpha^s[\alpha]$ from **Paper B** for three representations of the effective material on a hollow plane strain sheet similar to [45],

- **Plasticity** - a plasticity model with pure isotropic hardening.
- **Visco-Plasticity** - a visco-plastic model at iso-thermal conditions.
- **Thermo-Visco-Plasticity** - the full model containing all dependencies e.g. isotropic hardening, strain-rate and temperature.

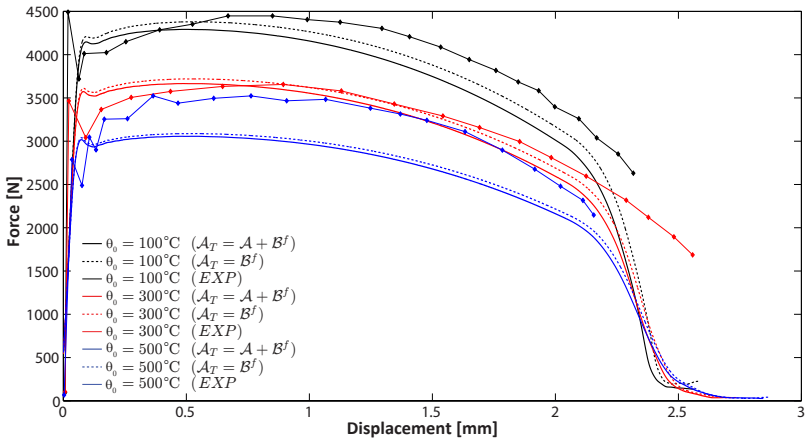

(a) *The influence of the total damage driving energy ($\mathcal{A}_T$) for a cylindrical test specimen having the initial temperatures 100 °C, 300 °C and 500 °C. The numerical results are compared to experimental data obtained from [77].*

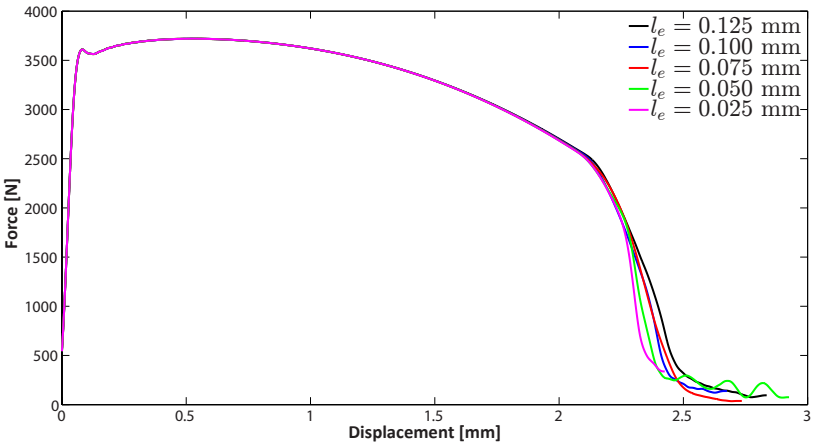

(b) *Mesh objectivity for a cylindrical test specimen using an initial temperature of 300 °C. The FE- discretizations range between $l_e = 0.125$ mm to $l_e = 0.025$ mm and the length scale parameter was set to $l_c = 0.125$ mm.*

Figure 3.8: *Force versus displacement response for a cylindrical test specimen for varying damage driving energy representations together with the effect on the mesh objectivity.*

Evidently, the void nucleation term is shown to have a stabilizing effect on the force versus displacement response. Moreover, the strain-rate dependence has a significant effect on the response compared to thermal softening for this specific example. The softening seen at higher temperatures is due to geometry changes possibly combined with strain softening.

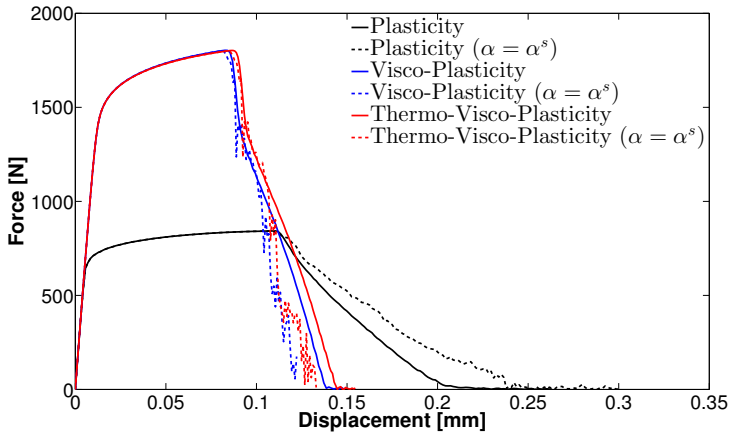

Figure 3.9: *Influence of strain rate and temperature in the response curve of the hollow plane strain sheet. For comparison, the corresponding response curves using the static damage evolution rule ($\alpha = \alpha^s$) are included, dotted lines.*

3.4.5 Influence of stress triaxiality and damage driving energy

The continuum damage modeling framework presented in section 3.4.3 is the approach adopted for the simulation and modeling of the machining process in **Paper D**. However, the stress triaxiality effect has been shown to be of significance in order to capture the material separation during the machining operation [75]. The proposed damage modeling framework is therefore validated in **Paper C** with respect to on the one hand varying stress triaxiality (notch intensity) and on the other the choice of damage driving energy $\mathcal{A}_T$. In particular, three different representations of the damage driving energy were considered in order to investigate how well they are able to capture the fracture process of tensile loaded notch specimen made of compacted graphite iron (CGI). The considered representations are,

- **Elastic Damage** (ED) - The total damage driving energy is represented by the elastically stored free energy in the effective material under the assumption of a completely elastic continuum response.
- **Plastic Damage** (PD) - The total damage driving energy has only inelastic contributions and an onset threshold of inelastic damage driving energy controlled by the JC fracture model.
- **Elasto-Plastic Damage** (EPD) - Assuming an elasto-plastic continuum response, the total damage driving energy has elastic and inelastic contributions and an onset threshold of inelastic damage driving energy controlled by the JC fracture model.

The different approaches were compared to results from experiments on a set of notched specimens, each representing a specific state of stress triaxiality, subjected to tensile loading under quasi-static and iso-thermal conditions. The considered notched specimen

and their influence on the failure strain are illustrated in Figure 3.10 where detailed dimensions of the shear notch specimen can be found in [78].

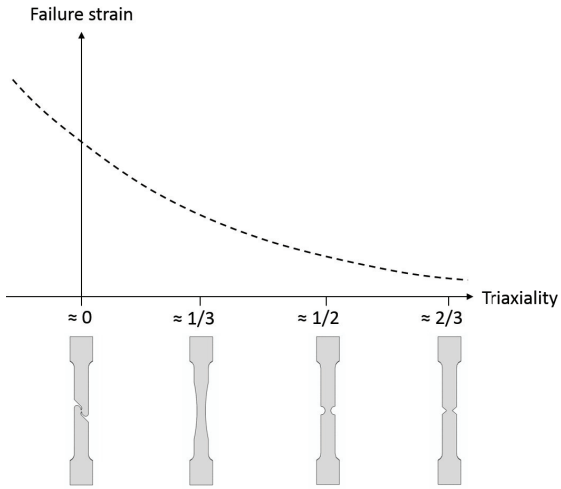

Figure 3.10: *The effect of triaxiality on failure strain for respective notch specimen.*

The considered CGI material is strongly heterogeneous consisting of three microstructural phases, graphite, pearlite and (small amounts of) ferrite though it is modelled as being homogeneous in **Paper C**. The graphite phase has a "worm" shape in 2D while in 3D the "worms" are interlaced with their nearest neighbour thus creating a complicated coral like morphology. This can be compared with gary iron (GI), where the graphite consists of partly flake like shapes with sharp edges causing an increased stress concentration and initiation of cracks at those sites hence, making the material brittle. Even though CGI is considered to be of naturally brittle character, its graphite morphology compared with the GI has been shown to increase the ductility of the material. In addition, the local strain levels accommodated by each phase in the CGI material are much larger than those measured globally [79]. This makes the CGI material a good choice for investigating the brittle-ductile behavior and to compare how different damage models may capture the fracture process recorded in [78].

The global force versus displacement response during the experimental tensile test was recorded for all notch specimen (5 experiments per notch) and can be seen in Figures 3.11-3.12. In addition to the experimental response, the numerical force versus displacement curves for each representation of the damage driving energy listed earlier are included in the figures. Even though CGI is regarded as relatively brittle material, it is seen that the ED approach, which might be considered as a representation of LEFM but without a pre-crack, is not sufficient enough to represent the force versus displacement response satisfactory. Evidently, the results indicate that the inelastic part of the damage driving energy is necessary in order to accurately predict the experimental force versus displacement response. Though an homogeneous representation of the CGI material is considered, the results imply that the inelastic deformations (strains), though small, are

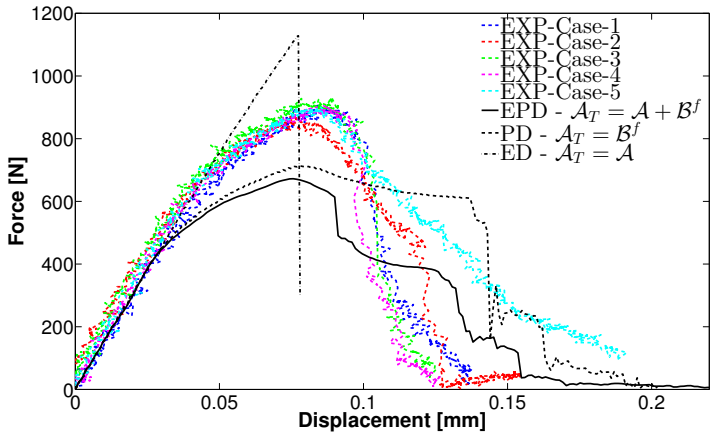

(a) *Shear notch specimen.*

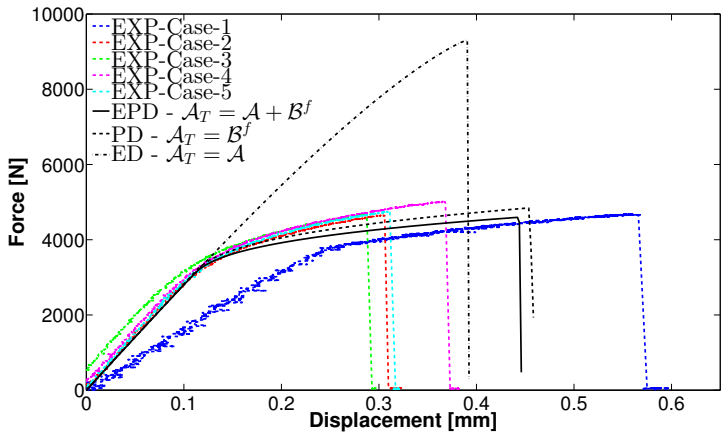

(b) *Smooth notch specimen.*

Figure 3.11: *Comparison between the numerical approaches against experimental force versus displacement results for the shear and smooth notch specimen, respectively.*

significant.

Furthermore, the stress triaxiality clearly affects the models ability to accurately capture the response. If the shear and triangular notch specimen are considered which correspond to the lowest and highest states of stress triaxiality, the adopted damage modeling is able to capture the response with respect to peak load and displacement to fracture. For the intermediate stress triaxiality cases, the agreement with the recorded force versus displacement curves is good for the peak force but less good for the maximum displacement. Note though the large spread in maximum displacement for the smooth notched specimen.

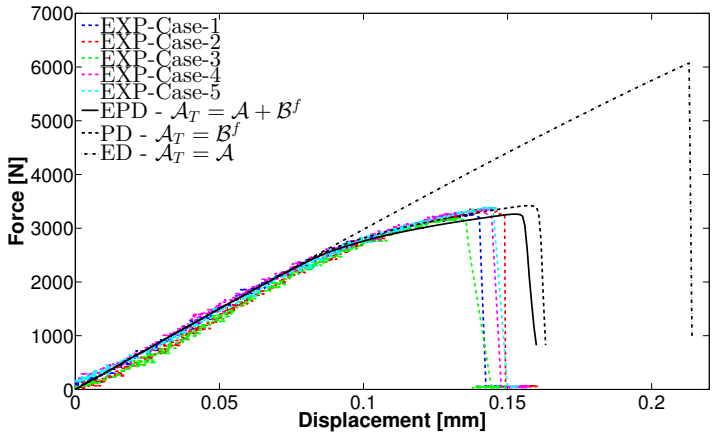

(a) *Circular notch specimen.*

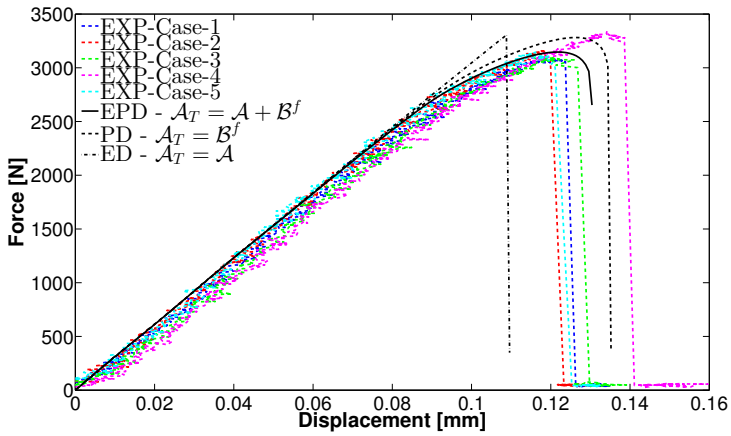

(b) *Triangular notch specimen.*

Figure 3.12: *Comparison between the numerical approaches against experimental force versus displacement results for the circular and triangular notch specimen, respectively.*

So, it should be highlighted that the force versus displacement response obtained by applying the PD and EPD representations of the damage driving energy for the circular notch specimen are able to capture the behavior in accordance to experimental results.

4 Modeling of the machining process

To represent the machining process from the modeling point of view, the fundamental mechanisms e.g. material flow, separation of surfaces, large strains and elevated temperature need to be captured by the modeling framework considered. The objective with the current section is to describe the modeling strategy adopted for the machining process, with emphasis on orthogonal cutting, and to highlight the main results presented in **Paper D**.

4.1 Nickel-based superalloy - Alloy 718

Nickel-based superalloys, such as Alloy 718 are often used in high temperature applications e.g. gas turbines, jet engines and space applications. The primary reason for the wide range of applications relate to its superior properties such as wear resistance, good corrosion and creep resistance alongside a preserved strength and hardness at elevated temperatures. However, the disadvantage is that these properties in combination with low thermal conductivity are partly responsible for the poor machinability of Alloy 718, thus often referred to as difficult-to-cut material [80].

Besides the poor machinability, shear localized (serrated) chips are formed when machining Alloy 718 at high cutting speeds which is often explained by the potential occurrence of adiabatic shear instability in the primary deformation zone [81]. Interestingly, when machining Alloy 718 at low cutting speeds a continuous chip morphology is manifested. The wide variety of chip formations with increasing cutting speed, seen in Figure 4.1, makes Alloy 718 a good candidate to validate the adopted modeling strategy for the representation of the orthogonal cutting process in the current work.

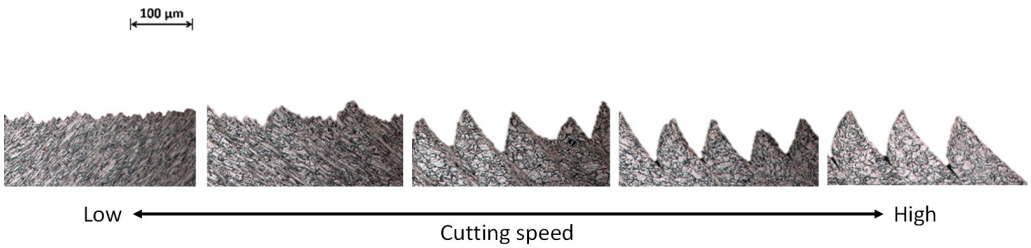

Figure 4.1: *The variation of chip morphology, of Alloy 718, with varying cutting speed from low (30 m/min) to high (480 m/min), from [82].*

4.2 Adopted modeling framework

The numerical modeling of the orthogonal cutting process herein, is achieved by applying the modeling strategy developed in section 3.4.3 into the commercial software DEFORM 2D ^{TM}. A Lagrangian framework is considered and combined with a continuous re-meshing technique. The separation of surfaces, creation of the chip and a control of the element distortion is resolved via the re-meshing scheme. To model the chip morphology during the machining of Alloy 718, the continuum damage modeling framework is introduced in a rigid visco-plastic flow formulation e.g. [83]. This implies that the inelastic contribution to the damage driving energy, introduced in Eq.(3.7), is assumed to promote the damage evolution after the damage threshold criterion is signaled thus $\mathcal{A}_T = \mathcal{B}^f$. It is a valid assumption for metal cutting simulations since the elastic contribution to the deformation is insignificant compared with the total amount of material deformation at the vicinity of the cutting tool.

The continuum material response, until the damage threshold criterion is reached, is governed by the visco-plastic Johnson-Cook constitutive model, presented in Eq.(3.3). In this work, the damage threshold criterion, signaling the initiation of the isotropic scalar damage evolution in this case, is represented by a modified version of the Cockcroft-Latham criterion [68] in terms of a damage initiation function $\phi_d[t]$. The damage initiation time $t = t_f$ is considered to be the time station when $\phi_d[t_f] = 0$ is fulfilled. The damage initiation function is thus postulated as

$$\phi_d = \hat{\mathcal{D}}^c_T[t] - W_{CL} \tag{4.1}$$

where W_{CL} is the so called Cockcroft-Latham damage parameter which represents the amount of dissipated energy needed for the onset of damage. Meanwhile, $\hat{\mathcal{D}}^c_T$ corresponds to the modified energy dissipation in terms of the effective mechanical dissipation in Eq.(3.4) simplified as $\hat{\mathcal{D}} = (\hat{\tau}_e - \hat{\kappa})\Delta\epsilon$. To account for the effect of stress triaxiality during the accumulation of $\hat{\mathcal{D}}^c_T$, it is assumed that damage is only promoted during tensile loading and suppressed otherwise. This is expressed as

$$\hat{\mathcal{D}}^c_T[t] = \int_0^t \hat{d}\, dt \ , \ \hat{d} = \begin{cases} \hat{\mathcal{D}} & \text{if } \tau_1 \geq 0 \\ 0 & \text{if } \tau_1 < 0 \end{cases} \tag{4.2}$$

where, τ_1 is the *maximum* principal stress of the Kirchhoff stress tensor and $\hat{d}$ is the effective mechanical dissipation rate at tensile loading.

So, when the damage threshold criterion is signaled, the continuum progressive ductile damage model (PDD), from section 3.4.3, successively degrades the effective flow stress until complete loss of material integrity is obtained. This model is compared with the common modeling approach where an instantaneous damage evolution (ID) is manifested upon reaching the damage threshold criterion. The material response is then suddenly degraded to a plateau representing $\zeta\hat{\tau}_y$ of the effective flow stress $\hat{\tau}_y$ and held fix throughout the simulation. In DEFORM 2D ^{TM}, the ID model is used to represent fracture. The use of the damage threshold criterion together with the degradation of the flow stress using the PDD and ID models is illustrated, in principal, in Figure 4.2.

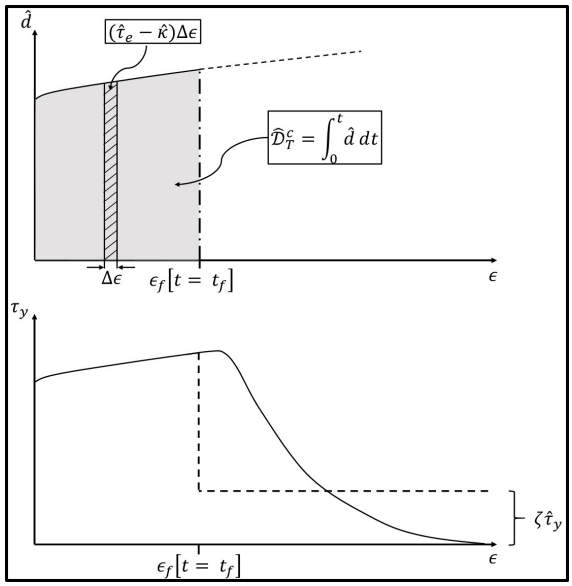

Figure 4.2: *Top) Representation of the onset threshold criteria for damage evolution. Bottom) Illustrates the PDD (solid) and ID (dashed) evolution laws.*

4.3 FE-modeling of machining

To represent the orthogonal cutting process in a FE context in DEFORM 2D ™the 2D modeling set-up for the coupled thermo-mechanical simulations is illustrated in Figure 4.3. The workpiece is assumed to be in horizontal motion, with the cutting speed v_c towards the tool, which was modelled as a rigid body. The mesh density of the workpiece and cutting tool is increased in the tool-chip interface to increase the accuracy of the solution and to improve the chip geometry.

Furthermore, a perfect thermal transfer is assumed at the contact regions between the tool-chip interface. This assumption was applied due to the high normal pressure in the tool-chip contact region. Even though the perfect thermal transfer assumption represent an ideal condition at the contact region, it is widely accepted for FE simulations of orthogonal machining e.g. [55], [80], [84].

In the current work, an existing pressure dependent shear friction model from [55] is used to describe the friction distribution at the tool-chip interface and is formulated as,

$$\tau_f = m_0 \left(1 - \exp[-\alpha_f p_c]\right) k_s \tag{4.3}$$

where τ_f represents the shear stress at the tool-chip interface, k_s is the shear strength of the workpiece material, p_c is the contact pressure while m_0 and α_f are friction coefficients representing the sticking-sliding frictional condition in the contact zone. This modeling representation of the stress distribution at the tool-chip interface indicate that the shear stress approaches the shear strength with increasing contact pressure. Meanwhile, as

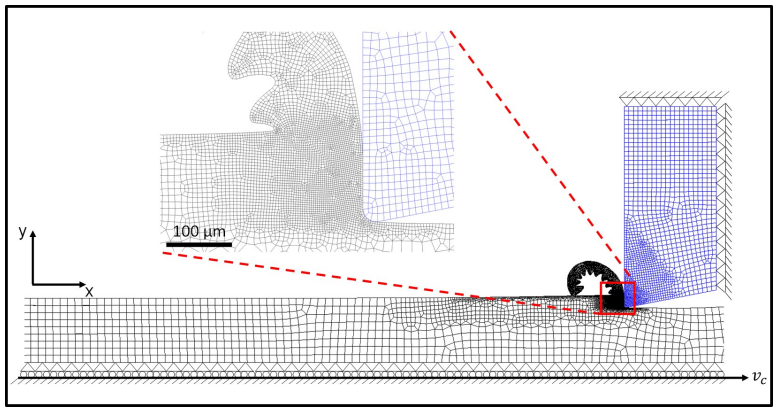

Figure 4.3: *The modeling set up used in DEFORM 2D^{TM}.*

the contact pressure decreases so does the shear stress thus potentially representing the sticking-sliding contact condition at this interface.

Finally, the PDD and ID model, the visco-plastic Johnson-Cook constitutive model, the pressure dependent shear friction model, the damage threshold criterion and the damage evolution law were implemented in DEFORM 2D ^{TM}by means of FORTRAN subroutines.

4.4 Machining simulation and experimental comparison

The current section summarizes the main results with respect to chip formation, cutting forces, contact lengths alongside the damage and temperature fields in **Paper D**. The orthogonal cutting process was simulated and experimentally conducted at different cutting speeds ranging from 30 m/min to 480 m/m with a constant feed rate of 0.1 mm/rev.

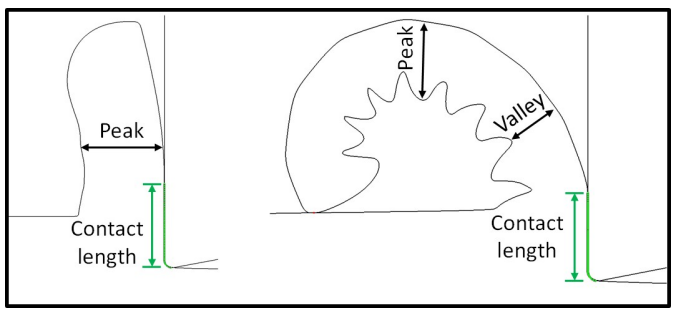

Figure 4.4: *Illustration of chip thickness measurements for continuous (left) and serrated (right) chip formation together with the contact length.*

The experimental transition from continuous to shear localized (serrated) chip formation was captured by both damage models (PDD and ID) at a cutting speed of 120 m/min. It was observed experimentally that the cutting and feed forces, chip thickness (both valley and peak seen in Figure 4.4) and contact length at the tool-chip interface decrease with an increasing cutting speed. The simulated results, independent of applied damage model, were in good overall agreement with the experimental observations. However, the difference between the simulated and experimental measurements for the highest cutting speeds (>120 m/min) with respect to the chip thickness (valley distance) and the cutting force successively increased. One may note, that in industrial machining applications of the Alloy 718 material, the cutting speed applied is normally very low. The highest cutting speeds (>120 m/min) in the current work, are primarily used to validate the model framework and identify its capabilities.

The increase in the relative difference between experimental and numerical results, for the higher cutting speed, could be related to the increased severity of the thermal and damage induced softening at the primary deformation zone. This is illustrated in Figure 4.6 for the ID and PDD model, respectively. Evidently, for speeds higher than the transitional cutting speed (120 m/min) the damage and the temperature fields localize in narrow bands in the primary deformation zone thus, initiating the formation of the shear localized chip formation. Interestingly, the severity of the damage increases with increasing cutting speed. This is manifested by the increasing depth of the damage zone, the distance it penetrates through the chip, while the width of this zone is successively reduced. Similar observations are captured experimentally in Figure 4.5, where microscopic fine level magnification images of the shear localized chip formation for the three highest cutting speeds are illustrated. Clearly, the width of the localized deformation zone is reduced while a pronounced crack formation is forming (indicated by a white arrow) with increasing cutting speed. These experimental observations and numerical results indicate that the shear localized chip formation, for Alloy 718, might be considered as a multi-mechanism process. For instance, at the transitional cutting speed micro-structural and thermal softening effects might be dominant while the effect of damage becomes increasingly significant at higher cutting speeds.

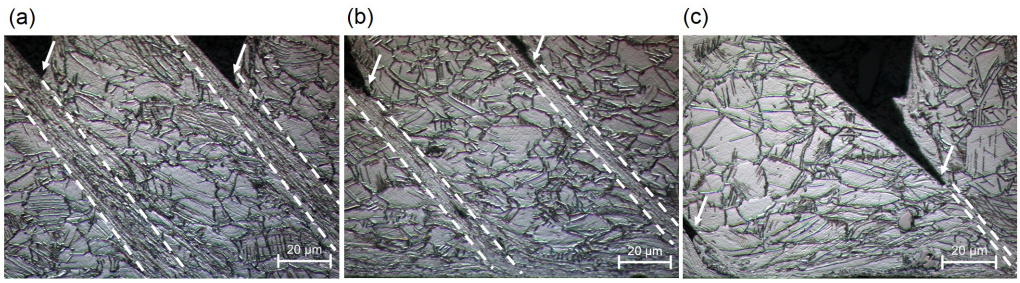

Figure 4.5: *The shear localized deformation zone for varying cutting speeds from [82] where a) v_c = 120 m/min, b) v_c = 240 m/min and c) v_c = 480 m/min.*

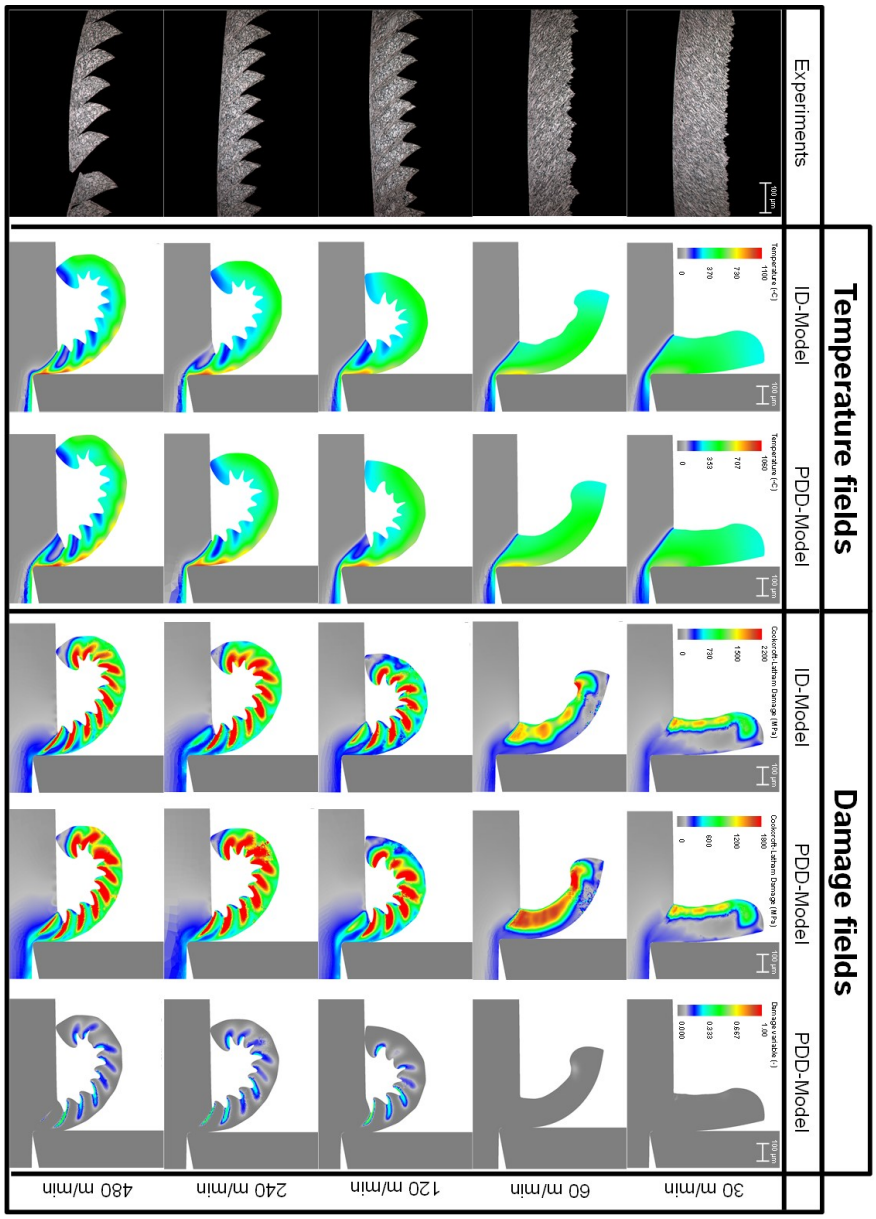

Figure 4.6: *Comparison between temperature and damage fields for respective modeling approach and varying cutting speeds together with the experimental chip formation from [82].*

5 Summary of appended papers

5.1 Paper A: Mesh objective continuum damage models for ductile fracture

The pathological mesh dependence related to the JC fracture model is investigated and a remedy to remove this behavior is proposed using two significantly different smeared damage models, presented in section 3.4.1 and referred to as the element removal and progressive damage model. By assuming that the damage field is "localized" within a single element width, the dissipated energy during the fracturing or rather damaging process should be consistent compared to a representative FE discretization. Thus, to secure that the same amount of dissipated energy is released, after onset of damage evolution and upon mesh refinement/coarsening, the proposed damage models are augmented with a mesh objective enhancement. To arrive at a mesh objective (mesh independent) smeared damage formulation, the local continuum framework is combined with concepts form the phase-field modeling e.g. the dissipation potential G. A key feature of the mesh objective enhancement is the introduction of the damage driving energy $\mathcal{A}_T$, relating the dissipation due to the continuously deforming material and the damaging process. Furthermore, the release of the damage driving energy is controlled by a damage threshold criterion based on the JC fracture model. Hence, by combining the principle of maximum dissipation with the dissipation potential during the damaging process a scaling factor is retrieved and applied in the damage law securing a consistent dissipation release.

The proposed mesh objective enhancement is investigated under shear deformation considering quasi-static and iso-thermal conditions. More precisely, the performance of respective damage model is studied with respect to the influence of mesh orientation on the mesh objectivity. When a structured mesh is applied, with respect to the loading direction, the progressive damage model is able to preserve the mesh objectivity, in view of the force versus displacement response. Moreover, the augmented element removal model can only retain a mesh objective response if a mesh refinement is applied relative to the reference mesh. The influence of unstructured mesh orientation was investigated based on a hat specimen from [76]. The damage models are shown to be able to capture representative damage modes. Also quantitatively, a good agreement is obtained for the effective stress and plastic strain levels. However, the damage patterns are not localized along one element width in this case independently of damage model, thus, there is a lack of clear convergence in the force versus displacement response.

5.2 Paper B: A ductile fracture model based on continuum thermodynamics and damage

A novel formulation for the representation of ductile material and fracturing response is presented. The formulations stems from a continuum thermodynamics point of view and is developed for the modeling and simulation of machining. In this context, a continuum

damage enhanced material formulation is applied to describe the material degradation in shear. The damage driving energy, part of the mechanical dissipation, is expressed such that it accounts for elastic and inelastic contributions. Hence, the initiation of the inelastic contribution is governed by a damage threshold criterion, based on the JC fracture model, controlling the amount of damage driving dissipation. Furthermore, the fracture area production is considered in terms of an area progression speed and a length-scale parameter without any non-local gradient term. In this way, the fracture area production is completely local, consisting of a damage induced convective part and a damage rate induced part.

The relevance of the damage threshold criterion is investigated where a uni-axial tensile test at material point level is considered. Here three different cases for the representation of the damage threshold criterion are assumed $t_f = 0$, $t_f = \infty$ and the one controlled by the JC fracture criterion. The results show that if $t_f = 0$ a purely elasto-plastic damage evolution and thus a brittle fracture. In contrast, $t_f = 0$ resembles a completely elastic damage while the JC fracture model is able to represent a more realistic ductile material response. In addition, results based on a hollow plane strain sheet subjected to tensile loading similar to [45] indicate that the proposed damage evolution law, including the damage rate induced contribution, stabilizes the response as compared to the use of a rate independent damage law. The influence of the area progression speed was shown to converge towards a finite value which might be thought to represent the damage propagation speed in the considered material. Additionally, it was shown in the validation example, from [77], where a pre-heated cylindrical specimen was subjected to tensile loading in a Split Hopkinson test, that the elastic damage driving energy has a small influence on the overall response compared to the inelastic counterpart. The mesh objectivity was shown to be preserved until the final stage of the loading process in the validation example where damage mode switching occurred depending on the degree of FE resolution.

5.3 Paper C: Validation of the ductile fracture modeling of CGI at quasi-static loading conditions

In this paper, the continuum damage model developed in **Paper B** is validated against experimental tensile loaded notched specimen of compacted graphite iron (CGI) material at quasi-static and iso-thermal conditions. As CGI is strongly heterogeneous material, consisting of pearlite, ferrite and graphit, it is naturally considered to be brittle due to the graphite content. However, it has been shown in [79] that the local strain levels accommodated by each phase in the CGI material are much larger than those measured globally. Therefore, the objective with the paper is to study the influence of the stress triaxiality effect, represented by the variations of notch specimen, on the fracturing process. In addition, three formulations for the mechanism of damage with respect to the damage driving energy are investigated and compared. The CGI material is modelled as homogeneous in the current paper.

During the experiments, force versus displacement curves together with the strain fields obtained using digital image correlation (DIC) analysis, were recorded. Experimental

results were compared with the numerical counterpart thus concluding that, even though CGI is considered naturally brittle, the inelastic contribution to the damage driving energy needs to be accounted for in order to accurately represent the material and fracturing response during the loading process. Furthermore, it is found that the level of stress concentration or stress triaxiality strongly affects the models ability to predict the force versus displacement response. Basically, with increasing stress concentration the model is clearly able to represent the experimental response more accurately than if the effect of stress concentration is negligible.

5.4 Paper D: FE modeling of machining Alloy 718 using a novel ductile damage model

In this paper, the developed framework for the representation of the ductile material and fracturing process in **Paper B** is applied to the modeling and simulation of machining e.g. orthogonal cutting. The main objective with the paper is to investigate the influence of damage and other micro-structural mechanisms on the chip formation process when machining Alloy 718 material which undergoes a transition from continuous to serrated chip formation with varying cutting speed. The phenomenological visco-plastic JC constitutive model is applied for the representation of the material response until damage initiation is signaled. The onset of damage evolution is controlled by a damage threshold criterion based on a modified version of the Cockcroft-Latham fracture criterion accounting for the effect of stress triaxiality. Whenever the damage threshold criterion is met, it is followed by a progressive damage evolution governed by the continuum damage law developed in **Paper B**. The modeling framework adopted e.g. the constitutive model, the damage threshold criterion and damage evolution law are implemented in a rigid-viscoplastic context in the commercial software DEFORM 2D ^{TM}via FORTRAN user subroutines. Furthermore, as a rigid-viscoplastic formulation is considered the damage evolution is assumed to be promoted by the inelastic deformation in the material only.

The performance of the proposed progressive ductile damage (PDD) modeling framework is compared with a more simplified approach where an instantaneous damage (ID) evolution occur after the damage threshold criterion is met. The FE simulation results are evaluated with respect to, chip morphology, forces and tool-chip contact lengths against experimental findings, obtained from orthogonal cutting tests at varying cutting speeds. An overall conclusion is that the proposed modeling framework is able to capture the chip formation, forces and tool-chip contact lengths in a good agreement with experimental measurements. Additionally, the transition from continuous to serrated chip formation is captured in excellent relation to the experimental observations. Furthermore, it is also shown that different mechanisms e.g. thermal, micro-structural and damage might influence the chip formation process at varying cutting speeds thus the need to account for these.

6 Conclusions

The present thesis work concerns the modeling of the ductile material response and fracture for FE simulations of the machining process. Thus, in the following the main results are summarized and discussed. In addition, an attempt is made to answer the posed research questions.

As the modeling framework will potentially be used in an industrial application for the optimization and increased understanding of the machining process, accuracy and robustness are key factors in order to succeed. To increase the accuracy of the modeling predictions, it is of utmost importance to understand the governing phenomena associated with ductile material behavior. Consequently, the ductile material response and fracture is frequently characterized with a significant amount of inelastic deformation where voids and micro-cracks nucleate, grow and coalesce on a micro-structural level to form macroscopic cracks. It is therefore, in machining, of significant interest that the modeling framework proposed can capture this response, including e.g. the creation of new surfaces and the chip formation. In addition, as machining is a rapid metal removal process, large inelastic strains, high strain-rates and elevated temperatures are an often occurring phenomena in the vicinity of the cutting tool edge and must also be accounted for.

Throughout the current work, **Paper A** - **Paper D**, the JC constitutive model for ductile materials has been applied for the representation of the visco-plastic material response. To capture the damage initiation and the ductile fracturing response, a combination of a damage threshold criterion followed by a damage evolution law is proposed in **Paper A** and **Paper B**. In particular, the need for a damage threshold criterion for the modeling of a ductile material response was illustrated in **Paper B**. The ductile material and damage modeling in the current work is derived within a thermodynamically consistent continuum framework. Thus, from the resulting dissipation rate, a damage driving energy is formulated based on elastic and inelastic contributions. Additionally, the damage threshold criterion, in **Paper A** - **Paper C**, is defined based on the JC fracture criterion, accounting for stress triaxiality, strain-rate and temperature dependency on the failure strain.

It is well known that continuum models e.g. use of the JC fracture criterion combined with deletion of elements tend to produce a pathological mesh dependent response. To remedy this inherited mesh dependence, a set of smeared damage models augmented with a mesh objective enhancement were proposed in **Paper A**. At quasi-static and isothermal conditions the damage models were shown to preserve a mesh objective response for structured FE discretizations. For unstructured meshes, however, the mesh objectivity could not be fully preserved. Concurrently, the damage models did capture realistic damage patterns, and also quantitatively, a good agreement was obtained for the effective stress and plastic strain levels compared to [76].

To be better suitable for machining simulations, the damage driving energy in the fracture modeling framework is formulated such that the damage evolution is promoted by shear deformation. Thus in **Paper B**, a progressive ductile damage evolution law is derived based on the balance between the damage driving energy and the damage induced fracture area production. The fracture area production consists of two terms modelling, in a physical fashion, the growth of voids and nucleation of new voids in a diffuse zone.

In addition, the inelastic part of the damage driving energy is activated when the damage threshold criterion is fulfilled while the elastic contribution is assumed to be initiated instantaneously. In this way, the progressive ductile damage model was shown to be able to capture the ductile material response and the subsequent fracture at high strain-rates and elevated temperature compared with experimental observations in [77] while partly preserving the mesh convergence. It is also shown how the two parameters in the in the fracture area production, v^* and l_c, who can be thought of as a measure of the area progression speed and the width of the diffuse zone respectively affects the response, and can be used to give a desired behavior. Furthermore, in order to properly capture the separation of surfaces and the subsequent chip formation during the machining process, it is well known that the state of stress at the vicinity of the cutting tool strongly affects this response [75]. Thus, in **Paper C** the ability of the model to capture the material response and fracture at various states of stress triaxiality is investigated. Evidently, a comparison with experiments showed that the progressive damage modeling framework is able to capture the fracture response as long as the inelastic part of the damage driving energy is included. It is also seen that the current model gives a much better agreement with experiments than the common method of element deletion with an improved control of the mesh dependency.

The progressive ductile damage model was applied for the simulation of orthogonal cutting in DEFORM 2D $^{\text{TM}}$under the assumption of rigid visco-plasticity in **Paper D** as a final step of this work. As for the damage threshold criterion, a modified version of the Cockcroft-Latham damage model was applied incorporating the effect of stress triaxiality. The difficult-to-cut material, Alloy 718, was considered for the workpiece material. The transition from continuous to serrated chip formation with increasing cutting speed made this material well suited for the validation and investigation of the proposed modeling framework. The simulation results were compared with experimentally determined forces, tool-chip contact-lengths and chip formations at varying cutting speeds with good agreement. The transitional cutting speed at which a transition from continuous to serrated chip formation occur, was also predicted correctly compared with experiments. In addition, it was shown experimentally and numerically that the width of the shear localized zone in the vicinity of the cutting tool decreases with an increasing cutting speed. This might indicate that the formation of serrated chip formation is a multi-mechanism process, where different mechanisms increase in significance at varying cutting speeds. The current model was found to give similar results as the instantaneous damage evolution model (standard in DEFORM 2D $^{\text{TM}}$) using roughly the same computational time and storage. However, the current model is believed to be physically more sound and have a better control of the mesh dependency, which for the commercial software DEFORM 2D $^{\text{TM}}$is controlled by mesh refinement. One may also note, that the choice of values for the parameters in the damage evolution, the resulting curve from the progressive model resembles almost the ID curve (Figure 4.2).

7 Future work

Despite the promising achievements presented in the present thesis, challenges exist which need to be addressed in order to further increase the efficiency, accuracy and robustness of the framework for modeling ductile fracture with damage evolution presented herein.

- Throughout the current work, the fracture energy release rate $\mathcal{G}_c$ was obtained based on the fracture toughness (from linear elastic fracture mechanics) for the material considered. However, one better representation of the fracture energy would be to use recorded instrumented Charpy-V tests [85]. Thus, in order to increase the accuracy of the modeling framework, conducting such experiments would be beneficial.

- In the damage evolution law, Eq.(3.16)-(3.18), the parameter l_c (figuratively the width of the diffuse zone in Figure 3.7), enters together with $\mathcal{G}_c$. It has been shown that l_c can be used to control the elastic damage driving energy $\mathcal{A}$ and thereby indirectly, in cases where $\mathcal{A}$ is omitted, cause a loss of thermodynamic consistency. Evidently, the use of l_c to model different levels of ductility and different shapes in the evolution of damage needs to be explored more.

- In order to further investigate and improve the mesh objectivity and better resolve the damage zone, the proposed modeling framework for ductile fracture and damage evolution response could be extended to incorporate gradient effects in the damage evolution law. Note though, that implementation of the damage model into commercial FE software will be difficult.

- The JC constitutive model applied for the representation of the visco-plastic material response is based on a multiplicative effect of strain hardening, strain-rate and thermal softening. It has, however, been shown that the model is not suited for high strain ranges and thereof fails to capture the high strain behavior which is often related to the flow softening phenomena. In addition, the JC constitutive model does not account for the coupling effects between the strain, strain-rate and temperature. In general, strain and strain-rate levels are much larger in the deformation zone during machining operations than those attained using e.g. the Split Hopkinson Pressure Bar test. Thus, to calibrate the flow stress response exceeding the experimentally obtained strain levels an extrapolation of the considered JC constitutive model is applied. This implies that, if the constitutive model considered is unable to account for various material or micro-structural effects at high strain levels e.g. dynamic strain-aging and re-crystalization the extrapolation might become incorrect. In line with these drawbacks, the constitutive model applied in the suggested modeling framework should potentially be reconsidered or the JC material model be modified.

- The CGI material in the current thesis was modeled as being homogenous even though it is strongly heterogeneous. Thus, to increase the accuracy on the modeling predictions of e.g. damage and strain levels these type of materials should be modeled as heterogeneous.

- Modeling of the tool wear was not part of the present thesis project even though it might strongly affect the overall machining response e.g. forces, surface integrity, chip formation and process stability among others. Therefore, it would be beneficial to incorporate the effects of tool wear in the proposed modeling framework.

References

[1] M. E. Merchant. Interpretive look at 20th century research on modelling of machining. *Machining Science and Technology* **2**.2 (1998), 157–163.

[2] T. Childs, K. Makawa, T. Obikawa, and Y. Yamane. *Metal machining: theory and applications*. John Wiley & Sons Inc. New York, NY, 2000.

[3] P. J. Arrazola, T. Özel, D. Umbrello, M. Davies, and I. Jawahir. Recent advances in modelling of metal machining processes. *CIRP Annals - Manufacturing technology* **62**.2 (2013), 695–718.

[4] J. Hashemi, A. A. Tseng, and P. C. Chou. Finite element modeling of segmental chip formation in high-speed orthogonal cutting. *Journal of Materials Engineering and Performance* **3**.5 (1994), 712–721.

[5] T. D. Marusich and M. Ortiz. Modeling and simulation of high speed machining. *International Journal for Numerical Methods in Engineering* **38**.21 (1995), 3675–3694.

[6] S. L. Soo and D. K. Aspinwal. Developments in modeling of metall cutting processes. *Proceedings of the Institution of Mechanical Engineers, Part L: Journal of Materials: Design and Applications* **221**.4 (2007), 197–211.

[7] G. Ljustina, R. Larsson, and M. Fagerström. A FE based machining simulation methodology accounting for cast iron microstructure. *Finite Elements in Analysis ad Design* **80** (2014), 1–10.

[8] M. Vaz, D. R. J. Owen, V. Kalhori, M. Lundblad, and L. E. Lindgren. Modeling and Simulation of Machining Processes. *Archives of Computational Methods in Engineering* **14**.2 (2007), 173–204.

[9] G. Ljustina. *Modeling of cast iron materials related to machining simulations*. PhD Thesis. Chalmers University of Technology, 2013.

[10] M. Ambati and H. Yuan. FEM mesh-dependence in cutting process simulations. *The International Journal of Advanced Manufacturing Technology* **53**.1–4 (2011), 313–323.

[11] J. Lemaitre. *A course on damage mechanics*. Springer-Verlag Berlin, 1996.

[12] M. A. Meyers and K. K. Chawla. *Mechanical behavior of materials*. Cambridge University Press. Cambridge, UK, 2009.

[13] F. A. McClintock. A criterion for ductile fracture by the growth of holes. *Journal of Applied Mechanics* **35**.2 (1968), 363–371.

[14] J. R. Rice and D. M. Tracey. On the ductile enlargement of voids in triaxial stress fields. *Journal of the Mechanics and Physics of Solids* **17**.3 (1969), 201–217.

[15] A. L. Gurson. Continuum theory of ductile rupture by void nucleation and growth: Part I—Yield criteria and flow rules for porous ductile media. *Journal of Engineering Materials and Technology* **99**.1 (1977), 2–15.

[16] V. Tvergaard. Influence of voids on shear band instabilities under plane strain conditions. *International Journal of Fracture* **17**.4 (1981), 389–407.

[17] G. Rousselier. Ductile fracture models and their potential in local approach of fracture. *Nuclear Engineering and Design* **105**.1 (1987), 97–111.

[18] A. Needleman and V. Tvergaard. An analysis of ductile rupture in notched bars. *Journal of the Mechanics and Physics of Solids* **32**.6 (1984), 461–490.

[19] T. Pardoen and J. W. Hutchinson. An extended model for void growth and coalescence. *Journal of the Mechanics and Physics of Solids* **48** (2000), 2467—2512.

[20] J. Lemaitre. A continuous damage mechanics model for ductile fracture. *Journal of Engineering Materials and Technology* **107**.1 (1985), 83—89.

[21] G. R. Johnson and W. H. Cook. "A constitutive model and data for metals subjected to large strains, high strain rates and high temperatures". *Proceedings 7th International Symposium on Ballistics*. Hague, The Netherlands, April 19–21, 1983.

[22] G. R. Johnson and W. H. Cook. Fracture characteristics of three metals subjected to various strains, strain rates, temperatures and pressures. *Engineering Fracture Mechanics* **21**.1 (1985), 31–48.

[23] Z. P. Bazant, T. B. Belytschko, and T. P. Chang. Continuum Theory for Strain-Softening. *Journal of Engineering Mechanics* **110**.12 (1984), 1666—1692.

[24] Z. P. Bazant and G. Pijaudier-Cabot. Nonlocal continuum damage, localization instability and convergence. *Journal of Applied Mechanics* **55**.2 (1988), 287—293.

[25] V. Tvergaard and A. Needleman. Nonlocal effects on localizaion in a void-sheet. *International Journal of Solids and Structures* **34**.18 (1997), 2221–2238.

[26] F. Reusch, B. Svendsen, and D. Klingbeil. Local and non-local Gurson-based ductile damage and failure modelling at large deformation. *European Journal of Mechanics A/Solids* **22** (2003), 779—792.

[27] D. S. Dugdale. Yielding of steel sheets containing slits. *Journal of the Mechanics and Physics of Solids* **8** (1960), 100–104.

[28] G. I. Barenblatt. Mathematical theory of equilibrium cracks in brittle fracture. *Advances in Applied Mechanics* **7** (1962), 55–129.

[29] R. Larsson, K. Runesson, and N. S. Ottosen. Discontinuous displacement approximation for capturing plastic localization. *International Journal for Numerical Methods in Engineering* **36**.12 (1993), 2087–2105.

[30] M. Ortiz, Y. Leroy, and A. Needleman. A finite element method for localized failure analysis. *Computer Methods in Applied Mechanics and Engineering* **61**.2 (1987), 189–214.

[31] A. Needleman. A continuum model for void nucleation by inclusion debonding. *Journal of Applied Mechanics* **54**.3 (1987), 525–531.

[32] M. Ortiz and A. Pandolfi. Finite-deformation irreversible cohesive elements for three-dimensional crack-propagation analysis. *International Journal for Numerical Methods in Engineering* **44**.9 (1999), 1267–1282.

[33] I. Scheider. Micromechanical based derivation of traction-separation laws for cohesive model simulations. *Procedia Engineering* **1**.1 (2009), 17–21.

[34] J. J. Remmers, R. de Borst, and A. Needleman. A cohesive segments method for the simulation of crack growth. *Computational Mechanics* **31**.1–2 (2003), 69–77.

[35] I. Scheider and W. Brocks. Simulation of cup–cone fracture using the cohesive model. *Engineering Fracture Mechanics* **70**.14 (2003), 1943–1961.

[36] T. Belytschko and T. Black. Elastic crack growth in finite elements with minimal remeshing. *International Journal for Numerical Methods in Engineering* **45** (1999), 601–620.

[37] J. M. Melenk and I. Babuška. The partition of unity finite element method: Basic theory and applications. *Computer Methods in Applied Mechanics and Engineering* **139**.1–4 (1996), 289–314.

[38] N. Moes, J. Dolbow, and T. Belytschko. A finite element method for crack growth without remeshing. *International Journal for Numerical Methods in Engineering* **46**.1 (1999), 131–150.

[39] G. Zi and T. Belytschko. New crack-tip elements for XFEM and applications to cohesive cracks. *International Journal for Numerical Methods in Engineering* **57**.15 (2003), 2221–2240.

[40] R. Larsson and M. Fagerström. A framework for fracture modelling based on the material forces concept with XFEM kinematics. *International Journal for Numerical Methods in Engineering* **62** (2005), 1763–1788.

[41] M. Fagerström and R. Larsson. Theory and numerics for finite deformation fracture modelling using strong discontinuities. *International Journal for Numerical Methods in Engineering* **66** (2006), 911–948.

[42] E. Svenning. *Multiscale modeling of ductile fracture in solids*. PhD Thesis. Chalmers University of Technology, 2017.

[43] C. Miehe, F. Welschinger, and M. Hofacker. Thermodynamically consistent phase-field models of fracture: Variational principles and multi-field FE implementations. *International Journal for Numerical Methods in Engineering* **83** (2010), 1273–1311.

[44] C. Miehe, M. Hofacker, and F. Welschinger. A phase field model for rate-independent crack propagation: Robust algorithmic implementation based on operator splits. *Computer Methods in Applied Mechanics and Engineering* **199** (2010), 2765–2778.

[45] C. Miehe, M. Hofacker, L. Schanzel, and F. Aldakheel. Phase field modeling of fracture in multi-physics problems. Part II. Coupled brittle-to-ductile failure criteria and crack propagation in thermo-elastic–plastic solids. *Computer Methods in Applied Mechanics and Engineering* **294** (2015), 486–522.

[46] M. Ambati, T. Gerasimov, and L. D. Lorenzis. Phase-field modeling of ductile fracture. *Computational Mechanics* **55**.5 (2015), 1017–1040.

[47] E. M. Trent and P. K. Wright. *Metal cutting*. Butterworth-Heinemann. Woburn, MA, 2000.

[48] N. H. Cook. "Chip formation in machining titanium". *Proceedings of the symposium on machine grind*. Watertown Arsenal, MA, 1953.

[49] M. C. Shaw, S. O. Dirke, P. A. Smith, N. H. Cook, E. G. Loewen, and C. T. Yang. *Machining titanium*. Tech. rep. Massachusetts Institute of Technology, 1954.

[50] M. C. Shaw and A. Vyas. Chip Formation in the Machining of Hardened Steel. *CIRP Annals* **42**.1 (1993), 29–33.

[51] A. Vyas and M. C. Shaw. Mechanics of Saw-Tooth Chip Formation in Metal Cutting. *Journal of Manufacturing Science and Engineering* **122**.2 (1999), p.10.

[52] G. ljustina, R. Larsson, and M. Fagerström. A FE based machining simulation methodology accounting for cast iron microstructure. *Finite Elements in Analysis and Design* **80** (2014), 1–10.

[53] M. E. Merchant. Mechanics of the metal cutting process II: Plasticity conditions in orthogonal cutting. *Journal of Applied Physics* **16** (1945), 318–324.

[54] P. L. B. Oxley. An analysis of orthogonal cutting with restricted tool-contact. *International Journal of Mechanical Sciences* **4** (1962), 129–135.

[55] A. Malakizadi, S. Cedergren, S. E. Ibrahim, and L. Nyborg. Inverse identification of flow stress in metal cutting process using Response Surface Methodology. *Simulation Modelling Practice and Theory* **60** (2016), 40–53.

[56] T. Shirakasi and E. Usui. "Simulation analysis of orthogonal metal cutting mechanism". *Proceedings of the first international conference on production engineering*, Part I. 1974.

[57] T. Ozel. The influence of friction models on finite element simulations of machining. *International Journal of Machine Tools and Manufacture* **46**.5 (2006), 518–530.

[58] L. Olovsson, L. Nilsson, and K. Simonsson. An ALE formulation for the solution of two-dimensional metal cutting problems. *Computers and Structures* **72** (1999), 497–507.

[59] M. R. Movahhedy, M. S. Gadala, and Y. Altintas. FE Modeling of Chip Formation in Orthogonal Metal Cutting Process: An ALE Approach. *Machining Science and Technology* **4** (2000), 15–47.

[60] T. Ozel and E. Zeren. Finite element modeling the influence of edge roundness on the stress and temperature fields induced by high-speed machining. *The International Journal of Advanced Manufacturing Technology* **34**.3–4 (2007), 255–267.

[61] M. Sima and T. Özel. Modified material constitutive models for serrated chip formation simulations and experimental validation in machining of titanium alloy Ti–6Al–4V. *International Journalof Machine Tools and Manufacture* **50** (2010), 943–960.

[62] F. J. Zerilli and R. W. Armstrong. Dislocation-mechanics-based constitutive relations for material dynamics calculations. *Journal of Applied Physics* **61**.5 (1986), 1816–1825.

[63] S. Buchkremer, B. Wu, D. Lung, S. Münstermann, F. Klocke, and W. Bleck. FE-simulation of machining processes with a new material model. *Journal of Materials Processing Technology* **214** (2014), 599–611.

[64] D. Umbrello, S. Rizzuti, J. Outeiro, R. Shivpuri, and R. M'Saoubi. Hardness-based flow stress for numerical simulation of hard machining AISI H13 tool steel. *Journal of Materials Processing Technology* **199**.1 (2008), 64–73.

[65] L. E. Lindgren, K. Domkin, and S. Hansson. Dislocations, vacancies and solute diffusion in physical based plasticity model for AISI 316L. *Mechanics of Materials* **40** (2008), 907–919.

[66] D. Wedberg and L. E. Lindgren. Modelling flow stress of AISI 316L at high strain rates. *Mechanics of Materials* **91** (2015), 194–207.

[67] S. N. Melkote, R. Liu, P. Fernandez-Zelaia, and T. Marusich. A physically based constitutive model for simulation of segmented chip formation in orthogonal cutting of commercially pure titanium. *CIRP Annals* **64**.1 (2015), 65–68.

[68] M. G. Cockcroft and D. J. Latham. Ductility and the Workability of Metals. *Journal of the Institute of Metals* **96** (1968), 33–39.

[69] Z. C. Lin and S. Y. Lin. A coupled finite element model of thermo-elastic-plastic large deformation for orthogonal cutting. *Journal of Engineering Materials and Technology* **114**.2 (1992), 218–226.

[70] R. Liu, S. Melkote, R. Pucha, J. Morehouse, X. Man, and T. Marusich. An enhanced constitutive material model for machining of Ti–6Al–4V alloy. *Journal of Materials Processing Technology* **213**.12 (2013), 2238–2246.

[71] T. Mabrouki et al. Some insights on the modelling of chip formation and its morphology during metal cutting operations. *Comptes Rendus Mecanique* **344**.4–5 (2016), 335–354.

[72] M. H Miguelez, X. Soldani, and A. Molinari. Analysis of adiabatic shear banding in orthogonal cutting of Ti alloy. *International Journal of Mechanical Sciences* **75** (2013), 212–222.

[73] O. Abiri and L. E. Lindgren. Non-local damage models in manufacturing simulations. *European Journal of Mechanics A/Solids* **49** (2015), 548–560.

[74] C. Hortig. *Local and non-local thermomechanical modeling and finite-element simulation of high-speed cutting*. PhD Thesis. TU Dortmund, 2010.

[75] J. Lorentzon, N. Jarvstrat, and B. L. Josefson. Modelling chip formation of alloy 718. *Journal of Materials Processing Technology* 209 (2009), 4645–4653.

[76] X. Teng, T. Wierzbicki, and H. Couque. On the transition from adiabatic shear bands to fracture. *Mechanics of Materials* **39** (2007), 107–125.

[77] T. Borvik, O. S. Hopperstad, S. Dey, E. V. Pizzinato, M. Langseth, and C. Albertini. Strength and ductility of Weldox 460 E steel at high strain rates, elevated temperatures and various stress triaxialities. *Engineering Fracture Mechanics* **72** (2005), 1071–1087.

[78] P. Hellström and K. Olander. *Analysis and modeling of properties of Compacted Graphite Iron on a microstructural level*. Master's Thesis. Department of Applied Mechanics, Chalmers University of Technology, 2012.

[79] T. Sjögren, P. E. Persson, and P. Vomacka. Analysing the deformation behaviour of compacted graphite cast irons using digital image correlation techniques. *Key Engineering Materials* **457** (2011), 470–475.

[80] A. Jafarian, M. I. Ciaran, D. Umbrello, P. J. Arrazola, L. Filice, and H. Amirabadi. Finite element simulation of machining Inconel 7118 alloy including microstructure changes. *International Journal of Mechanical Sciences* 88 (2014), 110–121.

[81] R. Komanduri and Z. B. Hou. On thermoplastic shear instability in the machining of titanium alloy (Ti-6Al-4V). *Metallurgical and Material Transcripts A: Physical Metallurgy and Materials Science* **33**.9 (2002), 2995–3010.

[82] A. Hagberg and P. Malm. *Material deformation mechanisms during machining of superalloys*. Master's Thesis. Department of Materials and Manufacturing Technology, Chalmers University of Technology, 2010.

[83] S. Kobayashi, S. I. Oh, and T. Altan. *Metal forming and the finite-element method*. Oxford University Press. New York, 1989.

[84] E. Abboud, B. Shi, H. Attia, V. Thomson, and Y. Mebrahtu. Finite Element-based Modeling of Machining-induced Residual Stresses in Ti-6Al-4 V under Finish Turning Conditions. *Procedia CIRP* **8** (2013), 63–68.

[85] T. R. Wilshaw and A. S. Tetelman. *In Measurements of Mechanical Properties Part 2, Techniques of Metals Research, Vol 5, Part 2*. p 103. Wiley Interscience. New York, NY, 1971.